COPPER ISOTOPE COMPOSITIONS OF CENOZOIC MAFIC-INTERMEDIATE ROCKS OF THE NORTHERN GREAT BASIN AND SNAKE RIVER PLAIN (USA)

by

ANNASTACIA LIN MAYNARD

B.S., SUNY at Fredonia, 2014

A THESIS

submitted in partial fulfillment of the requirements for the degree

MASTER OF SCIENCE

Department of Geology
College of Arts and Sciences

KANSAS STATE UNIVERSITY
Manhattan, Kansas

2016

Approved by:

Major Professor
Dr. Matthew Brueseke

Abstract

Mid-Miocene epithermal Au-Ag ores of the northern Great Basin USA are related to magmatism associated with the inception of the Yellowstone hotspot. The geochemical chemical connection between these ores and spatially and temporally related volcanism is not well understood, but has been suggested (Kamenov, 2007; Saunders et al., 2015). These Cu- and Pb-isotope studies show that the ore and associated gangue minerals have different sources of Pb, which supports evidence that the metal(loids) originate from a deep magmatic source (Saunders et al., 2008). Cu isotopes as a tool for exploring linkages between ore deposits and related volcanic rocks is a new and evolving field. A suite of mid-Miocene Northern Great Basin (NGB) and Snake River Plain (SRP) volcanic rocks was analyzed by aquaregia leach for their δ^{65}Cu compositions. These samples have all been previously characterized and include basalts, trachybasalt, basaltic andesites, and basaltic trachyandesites that are representative of regional flood basalt magmatism and younger basalt eruptions in central Idaho. Included are rocks from the Santa Rosa-Calico volcanic field, NV (e.g., Buckskin-National district); Owyhee Mountains, ID (Silver City District); Midas, NV region, near Jarbidge, NV; and a locality proximal to Steens Mountain, OR. Also included are two Pleistocene basalts from the central Snake River plain unequivocally related to the Yellowstone hotspot volcanism (McKinney Basalt and Basalt of Flat Top Butte), and one Eocene basalt from the Owyhee Mountains that is related to pre-hotspot arc volcanism. International rock standards ranging from ultramafic to intermediate were also analyzed in this study for comparison.

Our new δ^{65}Cu data greatly expands the range of known Cu isotopic compositions for basalts, with values ranging from -0.84‰ to +2.61‰. These values overlap with the δ^{65}Cu of regional ores, further suggesting a link between the source(s) of the ores and the NGB rocks. The range of δ^{65}Cu values also overlaps with mantle rock values, suggesting that the Cu isotopic composition may be a signature derived from the mantle source. Fractionation mechanisms that cause such a broad range in Cu isotopes are still unclear but liquid-vapor transitions and mantle metasomatism are being explored. Furthermore, δ^{65}Cu values of international rock standards reported in this study did not agree with previously reported data (Archer and Vance, 2004; Bigalke et al., 2010; Moeller et al., 2012; Liu et al., 2014, 2015) suggesting that aquaregia leach may not be a preferable technique when analyzing volcanic rocks.

Table of Contents

List of Figures

List of Tables

List of Equations

Acknowledgements

I would first like to give a big thank you to my main advisor, Matt Brueseke. Thank you for taking me on as a student and sticking with me through all of the ups and downs of this project. You have taught me so much more than just lessons in geology over the past two years, I really can't thank you enough. Thank you to Pamela Kempton for also being a great advisor and helping me immensely with this project, especially during the times when I thought finishing would be impossible. Thank you for giving me the opportunity to attend such an esteemed university and giving me the tools I needed to be successful. These last two years would not have been possible without you. Thank you to Matt Kirk for serving on my committee and also being an amazing mentor and teacher, I always thoroughly enjoyed your classes!

A big thank you goes to Ryan Mathur at Juniata College for running the Cu isotope measurements on all of my samples, and for being such an instrumental part of this project. Thank you for all of your help with my research, posters, and answering all of my questions when I needed help. Thank you to the Geological Society of America, the Geological Society of Nevada, the KSU Geology Department, and the KSU Graduate School for helping to fund this project. Thank you to all of the GEOL 103 students that I've taught during my time here. A special thanks goes out to my Monday morning classes – you always made teaching at 7:30am much more enjoyable with your jokes, positivity, and willingness to learn. To all the friends I have made here in the geology department, thank you for always being supportive! Moving half-way across the country is a little bit easier when you have great friends to have fun with, laugh with, and vent to, so from the bottom of my heart, thank you! To Lori, the best department secretary anyone could ask for, thank you so much for all of your help over the last two years. Thank you to John, who always put a smile on my face and brightened up my day during my early mornings and late nights in Thompson Hall.

And finally, a huge thank you goes out to each and every one of my family members, especially my parents. Thank you for always being there for me through everything. Thanks for letting me spread my wings and move to Kansas to follow my dreams. Thank you for stepping back and letting me have my independence, but lighting a fire under me when I needed it (even when I didn't want to hear it). None of this would have been a possibility without your continued support and unconditional love. Thank you to my sisters for the long phone calls when I needed

to vent, felt homesick, or just needed to talk. You girls are my rock! There are numerous others that have had a hand in my success with this project and although there are too many to name I would like to extend my sincere thanks to all of you. I am so thankful for all of the support that I have received during my time here in Kansas.

Chapter 1 - Introduction

It is likely that most, if not all, of the large ore bodies with visible surface outcrops have already been discovered. This means that exploration geologists are now faced with the mission of identifying a surface marker that indicates an ore deposit concealed at depth. It is, therefore, more important than ever to understand and identify not only the processes that move and deposit metals but also the source of the metals in order to aid in this more complex mode of exploration. Cu isotope signatures of minerals and rocks associated with Cu-bearing ore deposits may not only be a powerful geochemical tool with which to investigate fluid pathways in ore deposits but can also provide a means to discover these hidden resources (Mathur et al., 2012).

In this study, we present new Cu-isotope data from 14 Northern Great Basin (NGB) volcanic rocks that are spatially and temporally associated with mid-Miocene epithermal ore deposits in the region. The aim is to gain a better understanding of the link between copper fractionation and ore genesis and help to shed light on the mechanisms that may be contributing to copper isotope fractionation.

Many studies have dealt with copper isotope fractionation in low-temperature aqueous environments (Maréchal et al., 1999; Zhu et al., 2002; Larson et al., 2003; Ehrlich et al., 2004; Mathur et al., 2005; Markl et al., 2006; Mathur et al., 2012; Saunders et al., 2015). Modern advances in mass spectrometry have substantially increased the accuracy and precision in measuring both isotopes (^{63}Cu and ^{65}Cu) concurrently, which has opened the door for continued work on understanding Cu isotope behavior in Earth materials. The fractionation of copper isotopes can be quite extensive; for example, in porphyry copper deposits the range of δ^{65}Cu values spans from 9.8‰ to -16.48‰ (Mathur et al., 2009). In chondritic meteorites, however, the maximum variation does not exceed 1.6‰ (Luck et al., 2003).

There are several likely explanations for the natural variation of copper isotope ratios, e.g., redox reactions, involvement of organisms, equilibrium processes, liquid-vapor separation, magmatic differentiation, subduction processes, and metasomatism (Maréchal et al., 1999; Zhu et al., 2000, 2002; Jiang et al., 2002; Larson et al., 2003; Graham et al., 2004; Rouxel et al., 2004; Ehrlich et al., 2004; Liu et al., 2015). The scientific community is in agreement that both inorganic and biological processes can cause significant variations in copper isotope ratios at low temperatures (Gale et al., 1999; Maréchal et al., 1999; Zhu et al., 2000, 2002; O'Nions and Zhu,

2002; Riuz et al., 2002; Maréchal and Albarede, 2002; Larson et al., 2003; Graham et al., 2004). According to Markl et al. (2006) and Luck et al. (2003) high temperature hydrothermal processes such as liquid vapor separation and primary mineral precipitation may be capable of altering copper isotope compositions, but these authors conclude that magmatic processes do not appear to produce significant fractionation. While high temperature Cu isotope fractionation processes are unclear, they likely center on liquid-vapor transitions (Larson et al., 2003) and potentially mantle metasomatism, and/or slab dehydration during subduction (Liu et al., 2015).

In a recent study by Liu et al. (2015) non-metasomatized mantle peridotites show a δ^{65}Cu isotope range of -0.19 to +0.28‰. In comparison, metasomatized mantle peridotites were found to have highly variable Cu concentrations and isotopic compositions (δ^{65}Cu ranging from -0.64 to +1.82‰). Such a large range of Cu isotopic compositions in metasomatized peridotites is not easily explained by high temperature processes such as mantle partial melting. It is likely that the positive or negative effects of Cu isotopic ratios in peridotites results from sulfide dissolution-breakdown or mineral precipitation caused by metasomatism. These two processes may result in contrasting Cu isotope fractionations and may explain the variation of δ^{65}Cu values in the metasomatized peridotites.

In previous studies it has been accepted that mantle-derived igneous rocks have an average δ^{65}Cu value close to zero (Zhu et al., 2000; Li et al., 2009; Savage et al., 2013). The Bulk Silicate Earth (BSE) average value for δ^{65}Cu has been estimated at +0.06 ± 0.20‰ (2SD) by Liu et al. (2015) based on non-metasomatized peridotites, and mantle-derived melts, such as mid-ocean ridge (MORB) and ocean island basalts (OIB). Compared with the BSE, the Cu isotopes in chondrites are more fractionated. Most chondrites are enriched in ^{63}Cu, with δ^{65}Cu ranging from -1.50 to -0.09‰ in carbonaceous chondrites and -0.51 to +0.10‰ in ordinary chondrites (Luck et al., 2003). MORBs and OIBs analyzed by Liu et al. (2015) have homogenous Cu isotopic compositions (+0.04 to +0.14‰ and -0.07 to +0.18‰, respectively); this contrasts with the larger range observed in arc basalts (-0.19 to +0.47‰) and continental basalts (-0.18 to +0.35‰).

A few studies have investigated the link between copper isotopes and various ore deposits with an emphasis on porphyry copper deposits and epithermal ores (Larson et al., 2003; Mathur et al., 2009; Mathur et al., 2012; Saunders et al., 2015). Here we focus on the Cu isotope compositions of mafic to intermediate volcanic rocks that erupted in the northern Great Basin,

which are spatially coincident with coeval ~16-14 Ma epithermal ore deposits (Fig. 1-1A). These low-sulfidation epithermal ores are associated with the formation of the Columbia River Basalt province and the inception of the Yellowstone hotspot track (Geist and Richards, 1993; Perkins and Nash, 2002; Camp and Ross, 2004; Kamenov, 2007; Saunders and Brueseke, 2012). Epithermal ore deposits can form in subduction-related volcanic arcs, post-subduction volcanic settings, and back-arc rift zones under relatively shallow, low-temperature conditions (Simmons et al., 2005; Richards 2009; Saunders and Brueseke 2012; Saunders et al., 2015). Based on H- and O-isotope studies, the ore-forming fluids in these systems are a combination of heated meteoric water (O'Neil et al., 1973; John et al., 2003; Simmons et al., 2005; Saunders et al., 2008; Saunders et al., 2015) and primary magmatic fluids (Matsuhisa and Aoki, 1994; Hayashi et al., 2000; Faure et al., 2002; Heinrich et al., 2004; Williams-Jones and Heinrich, 2004; Saunders et al., 2008; Saunders et al., 2015).

Debate still exists regarding the sources of ore-forming constituents in these shallow ores. Some models suggest that metals and sulfur are leached from surrounding country rock as hydrothermal fluids migrate through the subsurface, while others propose a deeper magmatic source for the metals and metalloids. Heinrich et al. (2004) and Williams-Jones and Heinrich (2005) suggested that vapor-phase transport of ore metals and sulfur from a deep magmatic setting to a shallow epithermal system can occur due to low-density magmatic fluids. This type of metal transport can be observed in modern volcanic fumaroles, where μm-sized native gold particles, along with other metallic phases, precipitate directly from volcanic emissions (Meeker et al., 1991; Fulignati and Sbrana, 1998; Taran et al., 2000; Yudovskaya et al., 2006). The epithermal ore metals of the NGB, however, were likely released via magmatic fluids exsolved at depth, based on Pb- and Re-Os-isotope data (Kamenov et al., 2007; Saunders et al., 2008, 2014) as well as more recent Cu isotope results (Saunders et al., 2015). These studies suggest that the Au and Ag are not derived from adjacent host rocks but from mafic magmatic sources instead. Specifically, Saunders et al. (2015) observed that the Pb isotope data show disequilibrium between the gold ore and the co-deposited adularia in the Miocene Sleeper deposit, NV. In particular, the silicate minerals have an elevated $^{207}Pb/^{204}Pb$ ratio, which suggests that the gangue minerals have been leached from local sedimentary or metamorphic rocks. The gold ore, on the other hand, shows a lower $^{207}Pb/^{204}Pb$ ratio that overlaps with regional flood basalts, indicating that the metals were likely derived from a deeper mafic magmatic source (Kamenov et

al., 2007; Saunders et al., 2015).

The sample set from this study includes volcanic rocks associated with many of these epithermal ores, one Eocene-age basalt that erupted in southwestern Idaho before the flood basalt volcanism and is likely subduction-related, two Pleistocene (0.05 to 0.33) Ma central Snake River Plain basalts, along with a suite of igneous rocks that are geochemically well-characterized international reference standards from the United States Geological Survey (USGS) (PCC-1, DNC-1, BHVO-1, AGV-1, BCR-2), Geological Survey of Japan (JB-1a, JB-3, JA-3, JA-2, JB-2, JGb-1), and French Geological Survey (BE-N) which have no association to the local ore deposits. The international standards were analyzed in order to determine data accuracy in comparison to previously reported Cu data. These new Cu isotope data will enable the assessment of whether there is a relationship between the epithermal ores and the spatially associated volcanism and, if a relationship exists, to explore its nature. These results can aid current and future exploration efforts, not only across the state of NV and in the northern Great Basin, but regionally, or even globally. Furthermore, the Cu isotope results of this study expand the range of documented Cu isotope variability from continental mafic and intermediate volcanic rocks.

NGB Au-Ag Epithermal Ores and Coeval Magmatism: Geologic Overview

Prior to the mid-Miocene, the Northern Great Basin and surrounding area were tectonically complex and the current geological framework was a manifestation of a long history of convergent margin processes, subsequent extension, and volcanism. Commencing at ~17 Ma in the Pacific Northwest USA, ~250,000 km^3 of tholeiitic basalts to slightly more evolved compositions erupted to form the Columbia River Basalt (CRB) group (Brueseke et al., 2007; Camp, 2013). Volcanism was widespread and included lavas erupted in northern Nevada and southeastern Oregon (e.g., Steens Basalt). Coeval with this event, bimodal basalt-rhyolite volcanism began near the western edge of the present day Snake River Plain-Yellowstone province (Brueseke et al., 2014). The most intense volcanism migrated to the northeast over time as the continent moved over a stationary sublithospheric heat source now located at Yellowstone. The Yellowstone-Snake River Plain system is, thus, an age-progression of rhyolitic volcanism, although its origin remains contested. Some observations have led to the conclusion that inception of the Yellowstone hotspot volcanism is associated with the ascending tail of a deep

mantle plume (Armstrong et al., 1975; Smith and Braile, 1994; Camp 1995; Pierce and Morgan, 2009), while others suggest a shallow mantle origin (Fouch, 2012; Kelbert et al., 2012). The simplest petrogenetic explanation for the NGB rocks, and the one adopted in this study, is that they represent mantle melting associated with the inception of the hotspot (e.g., plume head) and any subsequent crustal interaction. The two young samples from the central Snake River plain likely represent lithospheric mantle melts (Leeman et al., 2008) or melts formed via mixing between plume-source mantle and the Archaean WY craton lithosphere (Hanan et al., 2008).

Many of the Mid-Miocene volcanic systems in northern Nevada host Au-Ag epithermal ore deposits (Brueseke, 2010; Saunders et al., 2008; Mason et al., 2015). Some of these deposits coincide spatially with the northern Nevada rift and other similar extensional structures in northern Nevada (Ponce and Glen, 2002). Faulting and tilting caused fractures, which created pathways for ore-forming hydrothermal fluids (and magmas) to migrate (Ponce and Glen, 2002; Leavitt et al., 2004). Regardless of the origin of these ore-forming fluids, the source magma chamber likely provided the heat necessary to drive these hydrothermal systems, which allowed for the mineralization of high-grade veins to form in fault zones throughout the region (Leavitt et al., 2004). A model proposed by Saunders et al. (2008) explains the host-rock relationships and ore mineralogies of regional low sulfidation Au-Ag mineralization. In this model, metal(loids) in NGB ore deposits, which are all texturally similar, were carried to the surface in mantle-derived hydrothermal fluids, irrespective of the deposit host rock lithology or age.

More recent research suggests that subduction processes may cause partial melts from "fertile" mantle to form in the mantle, which can later ascend through the lithospheric crust and lead to ore formation (Richards, 2009; Saunders and Brueseke, 2012). The majority of porphyry Cu, Mo, Au and epithermal Au deposits are genetically related to magmas in arcs above active subduction zones. These deposits are therefore linked to the petrogenesis of arc magmas and derive their fundamental characteristics such as enrichment of alkalies and some metals and metalloids, from subduction zones (Richards, 2009). Arc magmas are formed when partial melting occurs in the metasomatized wedge of asthenospheric mantle between the subducting oceanic and overriding oceanic or continental plates (Ringwood, 1977; Richards, 2009). Basaltic magmas formed in this process ascend through the upper plate lithosphere plate and evolve to form hybridized andesitic magmas characterized by high oxidation states and high water contents (Richards, 2003). These characteristics are essential for the formation of magmatic-hydrothermal

ore deposits (Candela, 1992). It is also possible that a postsubduction mantle plume could produce isotopically and compositionally similar magmas by triggering partial melting of the re-fertilized lithospheric mantle, thus, contributing to volcanism and related epithermal ore formation (Saunders et al., 2015).

Regionally, not all of the volcanism in the area has associated mineralization (Fig. 1.1B) and this study analyzes both volcanic rocks spatially associated with mineralization and some that have no known local spatial association. A detailed connection between these ores and spatially and temporally related volcanism is not well understood but has been proposed by Saunders et al. (2008, 2015). Furthermore, Cu-, S-, and Pb-isotope data presented by Saunders et al. (2015) provide evidence that metals and metalloids in epithermal Au-Ag deposits are sourced from the deep mantle.

Behavior of Copper and Copper Isotopes

Copper is strongly chalcophile and has two isotopes, ^{63}Cu and ^{65}Cu, with abundances of 69.174% and 30.826%, respectively, in reference to the SRM-NIST 976 standard (Shields et al., 1964; Albarede, 2004). It is a base metal and is typically mined from chalcopyrite ($CuFeS_2$), chalcocite (Cu_2S), cuprite (Cu_2O), and malachite ($Cu_2CO_3(OH)_2$). Copper has two important oxidation states, Cu^+ and Cu^{2+}; due to an unpaired electron, Cu^{2+} is the most common oxidation state under highly oxidizing conditions (Albarede, 2004). However, Cu^{1+} is more common below the hematite-magnetite buffer (Core et al., 2005). In silicates, Cu^{2+} can substitute for Fe^{2+} and Mg^{2+} in octahedral sites but, because the energy preference for this substitution is small, Cu is not particularly abundant in major FeMg-silicates. Under highly oxidizing conditions, where Cu^{2+} is the dominant oxidation state, it will most likely enter spinel structures such as magnetite. However, when Cu takes on the 1+ valence state it has a tendency to enter silicate structures such as plagioclase, likely substituting for Na^+ (Core et al., 2005). For example, Cu-rich plagioclase is found in NGB Steens Basalt lavas (Hofmeister and Rossman, 1985). Cu also forms numerous sulfides (typically associated with Fe) as well as carbonates and hydroxides where Cu^{2+} and Cu^+ occupy tetrahedral or octahedral sites (Albarede, 2004). In Cl-rich solutions Cu isotopes are strongly fractioned, which may be due to a multinuclear configuration of the molecules (Maréchal and Albarede, 2002). Similarly, multinuclear Cu sulfide complexes suggest a similar possibility in sulfide-rich aqueous systems (Helz et al., 1993).

In the ocean waters, Cu concentration increases with depth, which indicates that it is being used by organisms at shallower depths and/or scavenged by settling particles (Boyle et al., 1977; Bruland, 1983; Bruland and Franks, 1983). Only minimal data exists for Cu isotopes in sediments. In a core sample taken from the Central Pacific Ocean, δ^{65}Cu values of deep-sea clay vary from -0.94‰ to -2.83‰ within the first 760cm (Albarede, 2004; Russell et al. 2003). Luck et al. (2003) states that Cu in meteorites is depleted in the heavier ^{65}Cu isotope with respect to Earth. Of the four subgroups of carbonaceous meteorites analyzed (CI, CM, CO, and CV), the CV meteorites were the most depleted in ^{65}Cu and also depleted in much of their volatile elements. In mafic and ultramafic rocks, Cu can also be hosted in sulfides and oxides. On average, MORBs will contain approximately 70 ppm of Cu (www.earthchem.org/petdb). The relationship between porphyry copper deposits and subduction zones has been recognized for many decades and studied extensively (Sillitoe, 1972). Stolper and Newman (1994) concluded that the fluids expelled by slab dehydration during subduction are enriched in both Cu and Zn.

Copper behaves as a highly fluid-mobile element during slab dehydration in subduction zones (Liu et al., 2015), and studies suggest that over half of the Cu in subducted basaltic oceanic crust may be released during dehydration (Liu et al., 2015; Kogiso et al., 1997). Debate still exists about the mechanisms of Cu enrichment in copper porphyry deposits, most of which are hosted in subduction-related rocks. Mungall (2002) proposed that sulfide breakdown would result in an anomalously copper-rich source in the slab or mantle while others have proposed that the mantle and/or subducting slab do not contribute significantly to Cu enrichment but that enrichment is enhanced by magmatic differentiation processes within the crust instead (Lee et al., 2012; Chiaradia, 2014). Studying the Cu isotopes of low sulfidation Au-Ag deposits and copper porphyry deposits could be a useful tool in settling such a debate.

The fractionation of Cu isotopes has been documented in copper-rich minerals for over a decade (Maréchal et al., 1999; Zhu et al., 2002; Larson et al., 2003; Ehrlich et al., 2004; Mathur et al., 2005; Markl et al., 2006). Only recently has the geologic community begun to utilize Cu isotope fractionation processes as a tool for mineral exploration (Mathur et al, 2012; Mathur et al, 2010; Ponce and Glen, 2002; Saunders et al, 2015). It is likely that most copper isotope fractionation processes are occurring at low temperatures. However, it is still unclear how much high-temperature processes such as liquid-vapor transitions, mantle metasomatism, partial melting, and/ or slab dehydration during subduction contribute to Cu isotope fractionation

(Larson et al., 2003; Liu et al., 2015). In many porphyry copper and epithermal deposits, this liquid-vapor transition is a critically important part of the ore-forming process, because low-density fluids have the ability to transport ore metals and sulfur from a deep magmatic setting to the shallow crust (Heinrich et al., 2004; Williams-Jones and Heinrich, 2005; Saunders et al., 2015). Furthermore, Heinrich et al. (2004) and Williams-Jones and Heinrich (2005) proposed that vapor-phase transport of metals is the contributing factor for copper fractionation. Transport of metals by this process has been recorded in modern volcanic fumaroles, where μm-sized native gold particles, along with other metallic phases, precipitate directly from volcanic emissions (Meeker et al., 1991; Fulignati and Sbrana, 1998; Taran et al., 2000; Yudovskaya et al., 2006).

According to Liu et al. (2015) the Bulk Silicate Earth (BSE) has an average δ^{65}Cu value of +0.06 ± 0.20‰, thus Cu isotopic compositions for all mantle-derived rock types should cluster around 0‰. However, δ^{65}Cu values become fractionated to varying degrees in different lithologies (Table 1-1). Previous and current work show a limited range (-0.18‰ to +0.35‰), of copper isotope vales in continental basalts and a small dataset, i.e., n = 27 (Liu et al., 2015), thus it is important to expand the database of δ^{65}Cu values, particularly with respect to mafic rocks.

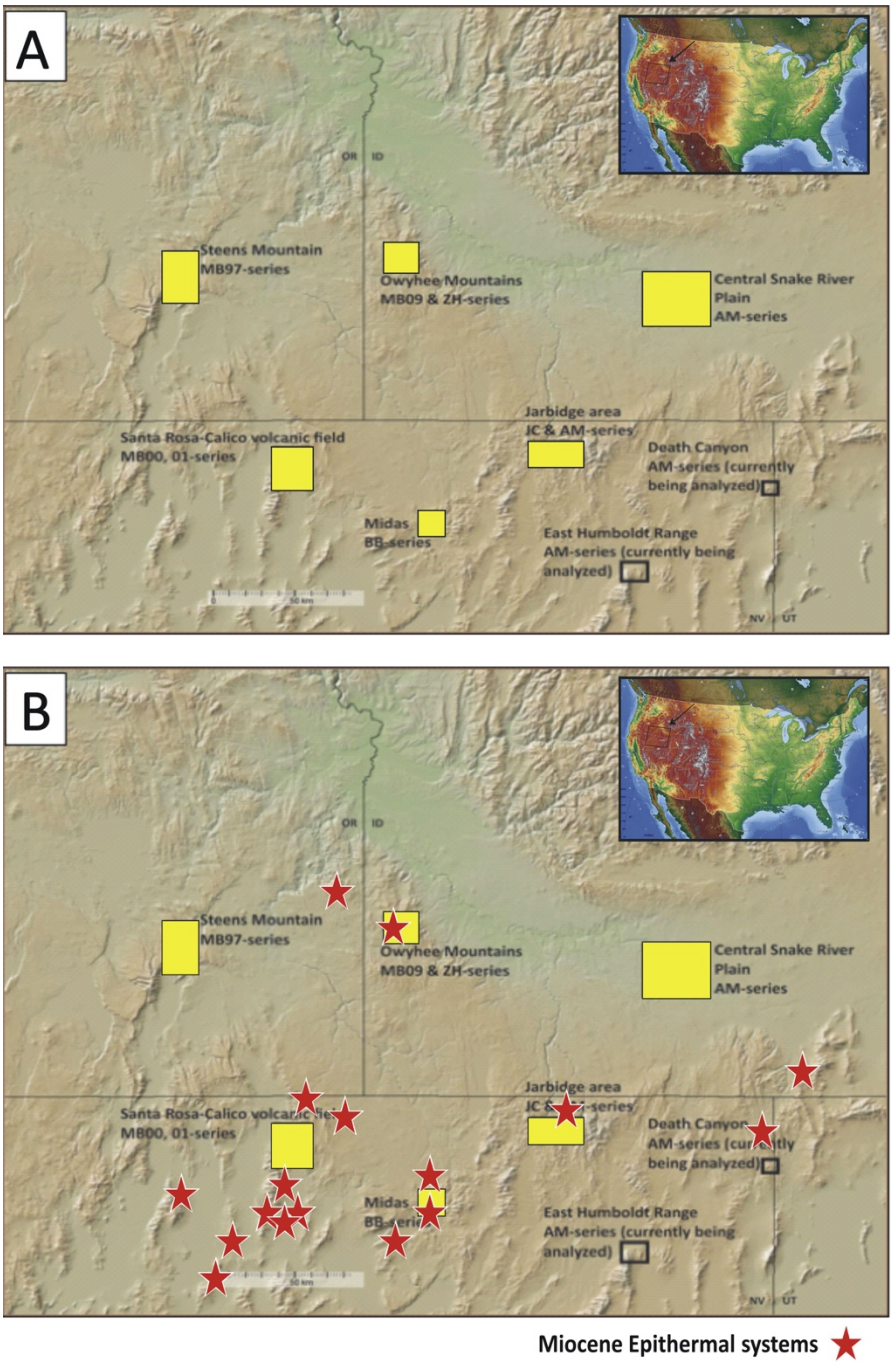

Figure 1-1 A) Map of the Northern Great Basin area. Digital elevation model showing the areas (outlined in boxes) where samples for this study were collected. B) Map of northern Great Basin area and associated Au-Ag deposits. Digital elevation model showing the epithermal deposits as yellow stars. Notice the close proximity of these deposits to come of the areas where samples were collected.

Table 1-1 Modified from Liu et al., 2015. Includes Cu isotope data from previously published work as well as new data on NGB rocks from this study. Values taken from Liu et al. (2015) are denoted with an asterix. Other previously published data include, metallic meteorites (Bishop et al., 2012), porphyry copper deposits (Li et al., 2010; Asadi et al., 2015), epithermal ores (Saunders et al., 2015), and granites; I- and S-type (Li et al., 2009).

Rock type/name	$\delta^{65}Cu_{range}$‰	$\delta^{65}Cu_{average}$‰	*2SD*	*N*
Cratonic peridotites* *(metasomatized)*	-0.64 to +0.68	0.11	0.52	23
Cratonic peridotites* *(non-metasomatized)*	-0.15 to +0.18	0.03	0.26	7
Orogenic peridotites* *(metasomatized)*	-0.34 to +1.82	0.02	0.6	10
Orogenic peridotites* *(non-metasomatized)*	-0.19 to +0.28	0.03	0.21	9
MORBs*	+0.04 to +0.14	0.09	0.08	6
OIBs*	-0.07 to +0.18	0.09	0.14	14
Continental basalts*	-0.18 to +0.35	0.1	0.24	27
Arc basalts*	-0.19 to +0.47	0.16	0.21	23
Andesites/dacites*	+0.04 to +0.38	0.11	0.21	70
NGB rocks *(from this study)*	-0.84 to +2.61	0.47	0.53	14
International rock standards *(from this study)*	-0.43 to +2.00	0.39	0.36	12
All basalts* *(previously published by Liu et al., 2015)*	-0.19 to +0.47	0.11	0.21	70
Metallic Meteorites	-2.26 to +0.99	-	-	-
Porphyry Cu deposits	-2.5 to +1.5	-	-	-
Epithermal ores	-2.5 to +3.5	0.24	0.28	37
I-type granites	-0.146 to +1.509	-	-	-
S-type granites	-0.463 to +0.205	-	-	-

Chapter 2 - Methods

Samples used in this study include: [1] a suite of Cenozoic volcanic rocks from the northern Great Basin and Snake River plain (U.S.A.) (Fig. 1-1) and [2] a suite of international rock standards (from the United States Geological Survey, Geological Survey of Japan, and French Geological Survey) that are primarily ultramafic to mafic in composition, but include three andesites, and are mostly volcanic, with the exception of one peridotite and one gabbro.

Cenozoic volcanic rocks were chosen from six different localities across northeastern Nevada, southeastern Oregon, and central and western Idaho (Fig 1-1a). Localities were chosen based on their proximity to coeval epithermal Au-Ag deposits. Bimodal basalt-rhyolite magmatism coupled with extension across Oregon, Washington, southwestern Idaho, and northern Nevada occurred ~16.7Ma. This led to a diversity of eruptive products and styles, including calderas and multiple discrete eruptive loci (Brueseke et al., 2014). Samples collected in the Owyhee mountains (MB09 & ZH series) were chosen based on the knowledge that these eruptive products and styles include locally emplaced epithermal Au-Ag ores that were transported from the mantle by mafic magmas. Major and trace element data for these rocks are reported in Hasten (2012). Local mafic volcanism in the Santa Rosa Calico volcanic field (SRC) was dominated by the eruption of the Steens Basalt magmas (Brueseke and Hart, 2008). Samples collected in the Steens Mountain area (MB97- series) (Brueseke et al., 2007) do not have any associated mineralization, but samples collected from the SRC area (MB00, 01 – series) do and are reported in Brueseke and Hart (2006). Only one sample collected from the Jarbidge Mountains region was used, and this data is reported in Brueseke et al. (2014). Data from samples collected near the Midas region in Nevada (BB-series) are unpublished, and major and trace element analysis procedures are discussed below. These rocks were collected directly from the Klondex-Midas mine site. The other rocks were collected from the central Snake River Plain (SRP). There are no known Au-Ag epithermal deposits in this region and these rocks were chosen to be used as a comparison with other basalt that are/are not related to mineralization. International rock standards are reported on the USGS, Geological Survey of Japan, and French Geological Survey websites.

Major and Trace Element Analysis by XRF and ICP-MS

Two newly collected samples (AM15-3, 4) from the central Snake River plain were split into smaller fist-sized fragments using a RockLabs Hydraulic Press equipped with tungsten jaws. Weathering rinds were removed from samples in a two-step process by, first, using a diamond-tipped blade rock saw to remove the outer surfaces. Any weathered material not removed during this process was removed by grinding the rock against a 60 grit, 8" silicon carbide (sandpaper) disc on a grinding wheel, then ground again to ensure each sample had no remaining flaws. All samples were then bathed with distilled water, cleaned thoroughly using a toothbrush, and allowed to air dry. Each sample was then crushed into pebble-sized pieces using the crushing jaws of the same RockLabs Hydraulic Press. These crushed samples were randomized using a cone-and-quarter method. A small amount of the crushed sample was powdered using a Spec Industries Shatterbox machine with aluminum ring and puck pulverizer. The powders were stored in glass vials in preparation for shipping for analysis. Major and trace element analysis was performed on these two samples and they were sent to Washington State University's GeoAnalytical Laboratory for X-ray Fluorescence and ICP-MS analysis.

The XRF analysis was done using a ThermoARL Advant'XP+ automated sequential wavelength spectrometer that measures 29 major and trace elements (Si, Al, Ti, Fe, Mn, Ca, Mg, K, Na, P, Sc, V, Ni, Cr, Ba, Sr, Zr, Y, Rb, Nb, Ga, Cu, Zn, Pb, La, Ce, Th, Nd, U). The ICP-MS analysis was done using an Agilent 7700 inductively coupled plasma mass spectrometer that measures 27 elements (14 REEs & Ba, Th, Nb, Y, Hf, Ta, U, Pb, Rb, Cs, Sr, Sc, Zr).

Geochemical analyses of the two BB samples were performed by ALS Geochemistry. The results of the analysis are previously unpublished (Brueseke pers. comm.). These rocks were collected from Midas NV at the Klondex Midas mine site and are sills unlike the other samples, which were lavas.

Samples picked for whole rock geochemistry were decomposed in a lithium metaborate/lithium tetraborate flux and mixed and fused in a furnace at 1000 ◦C. The melt was then cooled and dissolved in 100 mL of 4% nitric acid or 2% hydrochloric acid (HCL). The solution is then analyzed by inductively coupled plasma-atomic emission spectroscopy (ICP-AES) and reported as the percent oxide.

Trace element procedures for the BB samples are as follows. Prepared samples (0.25g) were digested with perchloric, nitric, hydrofluoric, and HCL. The residue is topped up with

dilute HCL and then analyzed by ICP-AES. Samples were digested with aqua regia for 45 minutes, cooled, and then diluted to 12.5 mL with de-ionized water. This solution was mixed and analyzed by inductively coupled plasma-mass spectrometry (ICP-MS). The analytical results were corrected for inter element spectral interferences. Samples (0.200g) were added to lithium metaborate flux (0.90g), mixed and fused in a furnace at 1000 °C. The melt was then cooled and dissolved in 100 mL of 4% nitric acid and analyzed by ICP-MS.

All samples with Fe values reported as FeO^T were corrected for oxidation and FeO and Fe_2O_3 were determined based on LeMaitre (1976). Mg# was calculated by following the method presented by Gill (2010):

$$\mathrm{Mg\#} = \frac{100\left(\frac{\mathrm{MgO}}{40.32}\right)}{\left(\frac{\mathrm{MgO}}{40.32}\right) + \left(\frac{\mathrm{FeO^T}}{71.85}\right)} \qquad \textbf{Equation 1}$$

Cu Isotope Analysis

Cu isotope analysis was completed at the University of Arizona on the multi-collector inductively coupled mass spectrometer (MC-ICP-MS) and the procedure closely follows that of Mathur et al. (2009). The samples are reported in delta notation in per mil relative to the NIST standard, as seen in the equation below.

$$\delta^{65}\mathrm{Cu}‰ = \left[\left[\frac{\frac{^{65}\mathrm{Cu}}{^{63}\mathrm{Cu}}\mathrm{sample}}{\frac{^{65}\mathrm{Cu}}{^{63}\mathrm{Cu}}\mathrm{standard}}\right] - 1\right] * 1000 \qquad \textbf{Equation 2}$$

Approximately 0.05g of rock powder were dissolved in 4mL of ultra-pure, twice-distilled aqua regia. Each aliquot was then dried and diluted in 6N HCl for column ion-exchange chromatography. The purification protocols are further described in Mathur et al. (2009). The column procedure separates copper from the remaining elements in the solute. The column procedure was performed twice on each aliquot and reported values from the analysis are an averaged value of the two measurements. Yields for the columns were checked volumetrically. The salts were then diluted to 200 ppb of copper in 2% HNO_3 and processed on the MC-ICP-MS. Because Ti oxides can cause direct interferences during measurement (Pribil et al., 2009), we monitored ^{49}Ti throughout the session and confirmed that Ti voltages were less than 10

millivolts, which is the background intensity observed on the Isoprobe. The standard bracketing method was used to correct for any mass bias from the Isoprobe. The NIST 976 standard was measured approximately 175 times throughout the analysis and the variation was measured at ± 0.14 ‰. (2SD).

Indices of alteration

Because of the potential for surface alteration processes to alter Cu-isotope compositions, estimates of the degree of alteration have been made using calculated chemical indices. The procedure used to calculate both the chemical index of alteration (CIA) and mafic index of alteration (MIA) parallels that used by Babechuk et al. (2014). The spreadsheet used to calculate the CIA and MIA values is in Babechuk et al. (2014). All major element oxides were first converted into moles of the oxide. CIA and MIA calculations were determined on NGB rocks collected for this study. The CIA is defined as

$$\mathrm{CIA} = \left(\frac{\mathrm{Al_2O_3}}{\mathrm{Al_2O_3} + \mathrm{Na_2O} + \mathrm{K_2O} + \mathrm{CaO^*}}\right) * 100 \qquad \textbf{Equation 3}$$

where CaO* represents only the silicate bound Ca and is therefor corrected for the presence of carbonate and apatite (Fedo et al., 1995).

$$\mathrm{CaO^*} = \mathrm{moles CaO} - \mathrm{moles CO_{2(calcite)}} - (0.5\mathrm{moles} * \mathrm{moles CO_2})_{(\mathrm{dolomite})} - \left[\left(\frac{10}{3}\right) * \mathrm{moles P_2O_5}\right]_{(\mathrm{apatite})}$$

Equation 4

CIA values were then plotted in A-CN-K space to determine the extent to which Ca, Na, and K are removed via surficial weathering (Fig.4-3).

The MIA is a chemical weathering index derived from the CIA and expanded to include the mafic elements Mg and Fe (Babechuk et al., 2014). There are two different equations for the MIA: 1) when the alteration environment is oxidizing and 2) when the alteration environment is reducing. In the first case Fe is retained, total iron is considered immobile along with Al_2O_3 and the MIA equation is:

$$\mathrm{MIA_{(O)}} = 100 * \left[\frac{\mathrm{Al_2O_3 + Fe_2O_{3(T)}}}{\mathrm{Al_2O_3 + Fe_2O_{3(T)} + MgO + CaO^* + Na_2O + K_2O}}\right] \qquad \textbf{Equation 5}$$

In the second case Fe and Mg are leached, total Fe, Mg, Ca, Na, and K are considered mobile elements and MIA equation is:

$$\mathrm{MIA_{(R)}} = 100 * \left[\frac{\mathrm{Al_2O_3}}{\mathrm{Al_2O_3 + Fe_2O_{3(T)} + MgO + CaO^* + Na_2O + K_2O}}\right] \qquad \textbf{Equation 6}$$

These values were then plotted on ternary diagrams in A-CN-K, A-CNKM-F, and A-CNK-FM space (Fig. 4-6, 4-8, 4-9, respectively).

Chapter 3 - Geochemistry and Cu Isotope Characteristics

Major elements are reported as weight percent oxide (wt. %) and trace elements as parts per million (ppm). The data for this study are reported in Appendix B.

Major Element Geochemistry

Cenozoic volcanics of the Northern Great Basin include basalts, basaltic andesites, trachybasalts, and basaltic trachyandesites, as shown on a total alkali vs. silica diagram (Fig. 3.1). The standards discussed in this study range from peridotites to andesites, the majority of which are mafic (Table 3-2). A list of all samples and their bulk major/trace element geochemistry is in Appendix B.

NBG rocks analyzed from this study along with two international rock standards (AGV-1 and BCR-2) have SiO_2 ranges between 47.38 and 55.49 wt. %. TiO_2 ranges from 0.82 to 3.33 wt. %; Al_2O_3 ranges from 13.97 to 17.54 wt. %; Fe_2O_3 ranges from 2.87 to 15.34 wt. %; MnO ranges from <0.01 to 0.22 wt. %; MgO ranges from 2.95 to 8.64 wt. %; CaO ranges from 5.78 to 11.22 wt. %; Na_2O ranges from 2.30 to 4.17 wt. %; K_2O ranges from 0.33 to 2.87 wt. %; P_2O_5 ranges from 0.14 to 5.17 wt. %, and Mg#'s range from 39.3 to 54.8. Weak negative relationships exist between Mg# and Na_2O and TiO_2 concentrations, while a positive relationship is observed with CaO (Fig 3.2). CaO, MgO, and total Fe_2O_3 also show a weak negative relationship with SiO_2 (Fig. 3.2). LOI's range from 0.00 to 8.47.

Almost all samples plot as tholeiitic on an AFM diagram (Irvine and Baragar, 1971) (Fig.3.4) with the exception of MB97-80, JC-09-20, and ZH11-4, which plot just under the calc-alkaline line. In general samples spatially and temporally associated with mineralization show a higher K/P ratio (Fig. 3.5) than those not associated with mineralization. Typically, mantle-derived rocks will have a ratio of 3.5 or below (Carlson and Hart, 1987), anything above this suggest that these rocks have been subjected to upper crustal contamination or extensive fractional crystallization.

Trace Element Geochemistry

Trace and rare earth element ranges for Cenozoic volcanics analyzed for this study exhibit the following ranges:

Table 3-1 Trace and rare earth element maximum and minimum values from NGB rocks are reported in parts per million

	Maximum	*Minimum*
Ba	1258	165.5
Cr	360	13
La	45	6.25
Rb	54	3.7
Sr	1505	232
V	463	166.39
Ga	27.8	16.8
Nb	24.9	3.2
Nd	54	11.15
Y	46	19.4
Zr	280.85	73.1
Sc	31.81	17.6
Cu	414	36.37
Ni	177	7
Pb	34.2	0.98
Zn	142	78

Some trace elements and REE's show a correlation with Mg# (Fig. 3.6), e.g., Ni and Cr increase with increasing Mg#.

Cu Isotope Results

The δ^{65}Cu values for NGB samples in this study range from -0.84 to +2.61‰ (Fig. 3.7). The international rock standards analyzed exhibit a much smaller range in values than the Cenozoic volcanics of the northern Great Basin and tend to have more positive values (Table 1-1). No correlations exist between δ^{65}Cu values and major element concentrations.

X-Y plots of δ^{65}Cu values vs. select metals (Fig. 3.8) show linear trends and relationships. Higher Ni concentration is weakly associated with higher δ^{65}Cu values ($r^2 = 0.30$), while higher Cu concentration weakly correspond to lower δ^{65}Cu values ($r^2 = 0.25$). Sr values tend to increase with increasing δ^{65}Cu values. In general, samples associated with mineralization have lower Zn concentrations that increase with increasing δ^{65}Cu values. These samples also display a trend of increasing V concentration as δ^{65}Cu values increase with the exception of the ZH11-4 sample that has the highest δ^{65}Cu value and lower V. REE's such as Dy, Sm, and Gd

exhibit a positive relationship with $\delta^{65}Cu$ values (Fig. 3-9) while Yb, Eu, and Lu do not show any correlation.

Table 3-2 Rock types listed for all samples used for this study including rock standards from the United States Geological Survey, Geological Survey of Japan, and French Geological Survey. Newly collected samples are denoted with an asterix.

Sample	Rock Type	Sample	Rock Type
MB00-30 B	Basaltic trachyandesite	Rock Standards	
MB01-12	Basalt		
MB09-13	Basalt	JB-1a	Basalt
MB09-29	Basalt	JB-3	Basalt
ZH11-4	Trachy-basalt	PCC-1	Peridotite
2-12BB	Basaltic andesite	JA-3	Andesite
6-12BB	Basaltic andesite	AGV-1	Andesite
JC-09-20	Basaltic andesite	JA-2	Andesite
MB97-74B	Trachy-basalt	BCR-2	Basalt
MB97-71	Basalt	JB-2	Basalt
MB97-80	Basaltic trachyandesite	BHV0-1	Basalt
MB97-31	Basalt	DNC-1	Diabase
AM15-3*	Basalt	JGb-1	Gabbro
AM15-4*	Basalt	BE-N	Basalt

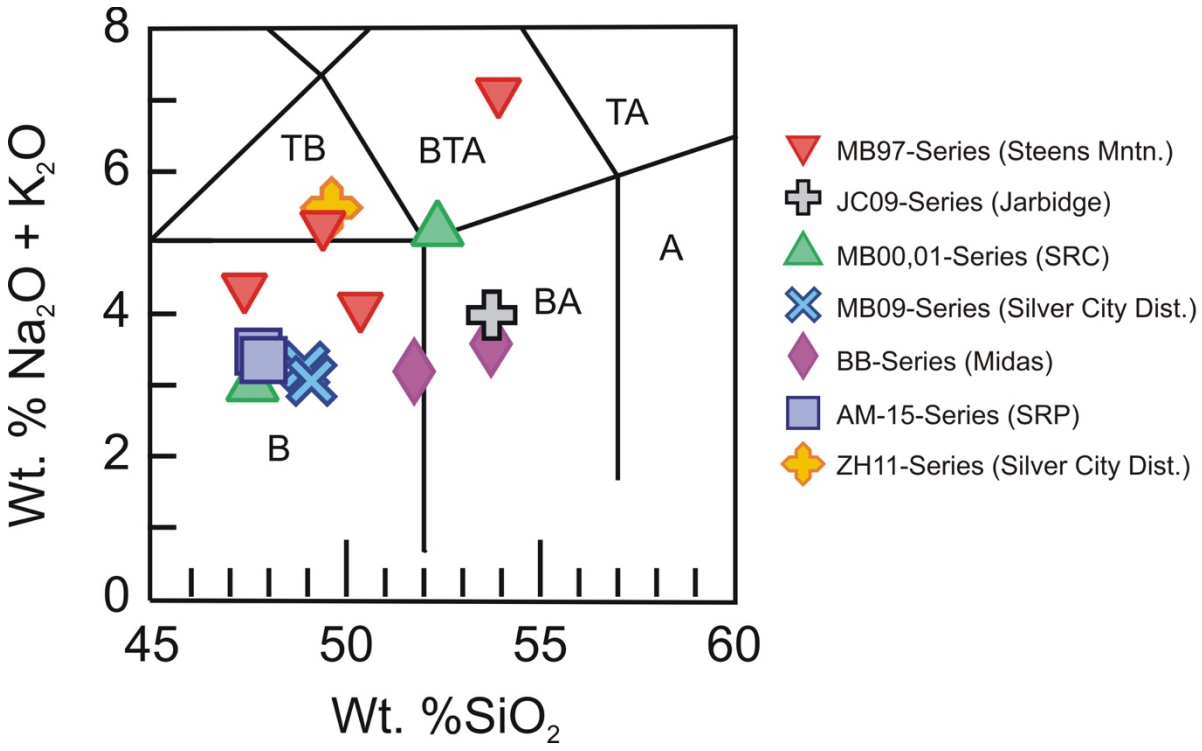

Figure 3-1: TAS diagram (LeBas et. al. 1986). Includes analyses from newly collected samples as well as previously collected samples. Notice that most samples plot as basalts, trachy-basalts, and basaltic andesites.

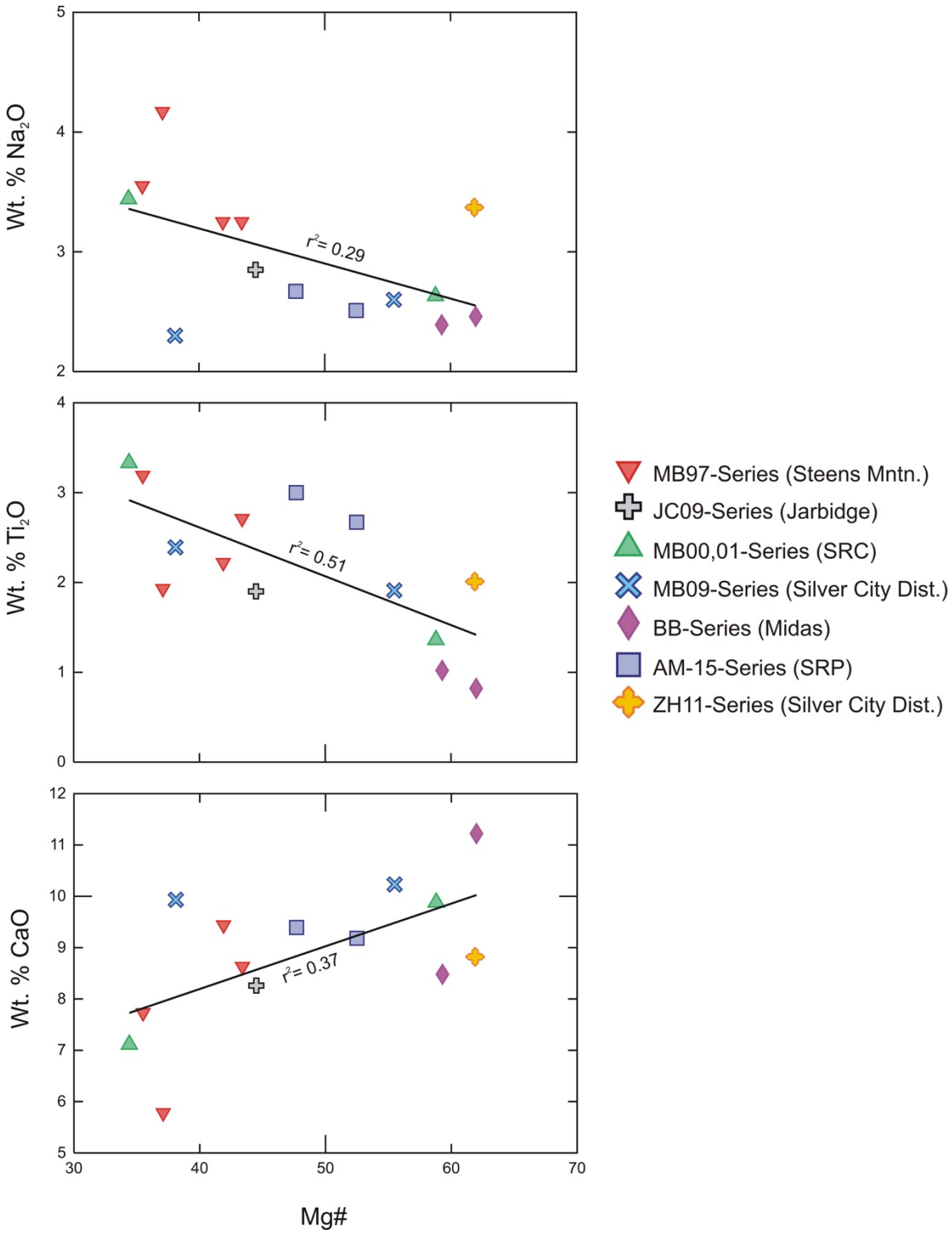

Figure 3-2: Major element oxides of NGB samples vs. Mg#. Notice the negative relationship between Na_2O and TiO_2 with Mg#, whereas CaO vs. Mg# exhibits a positive relationship.

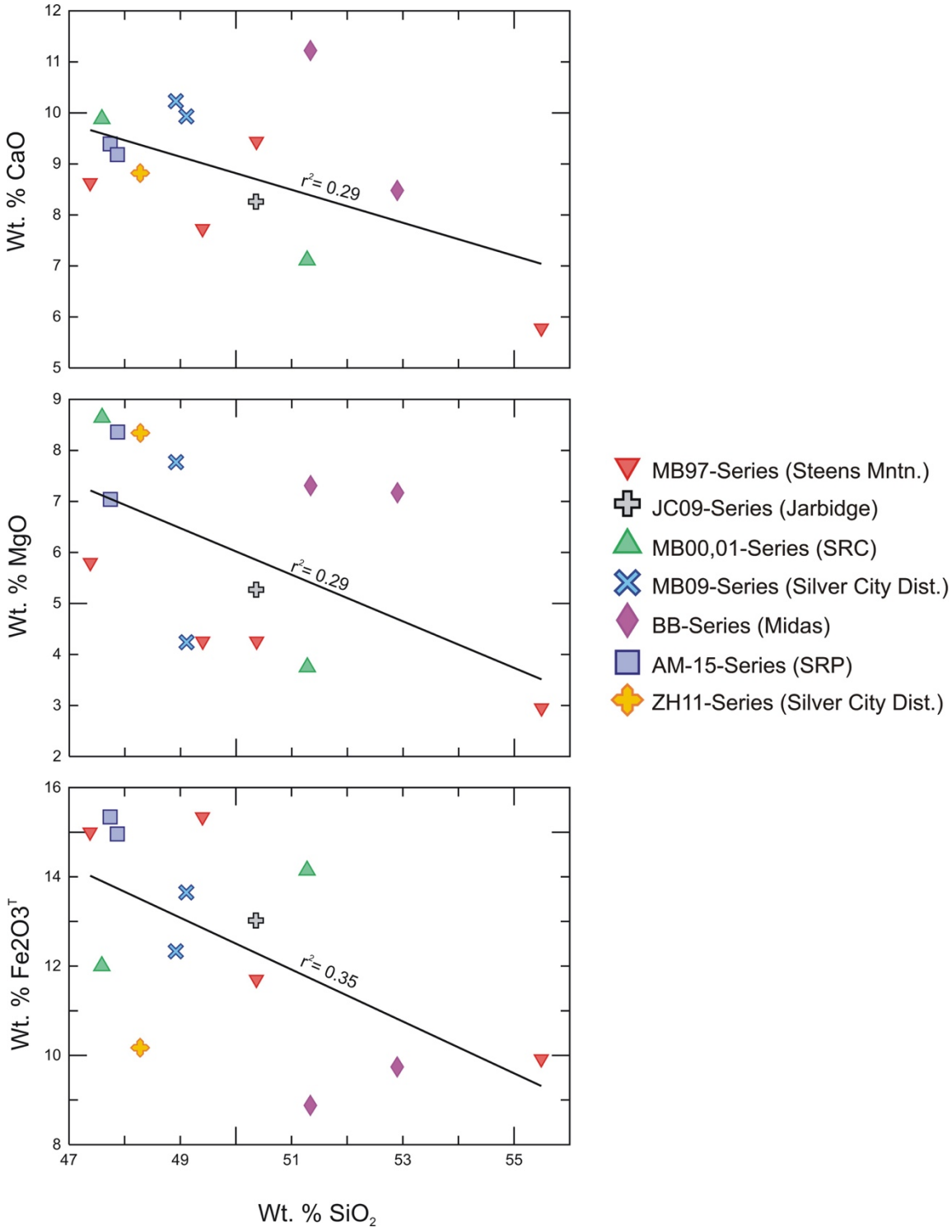

Figure 3-3: Major element oxides of NGB samples vs. wt. % SiO_2. Notice the negative trend between CaO, MgO, and total Fe_2O_3 with wt. % SiO_2.

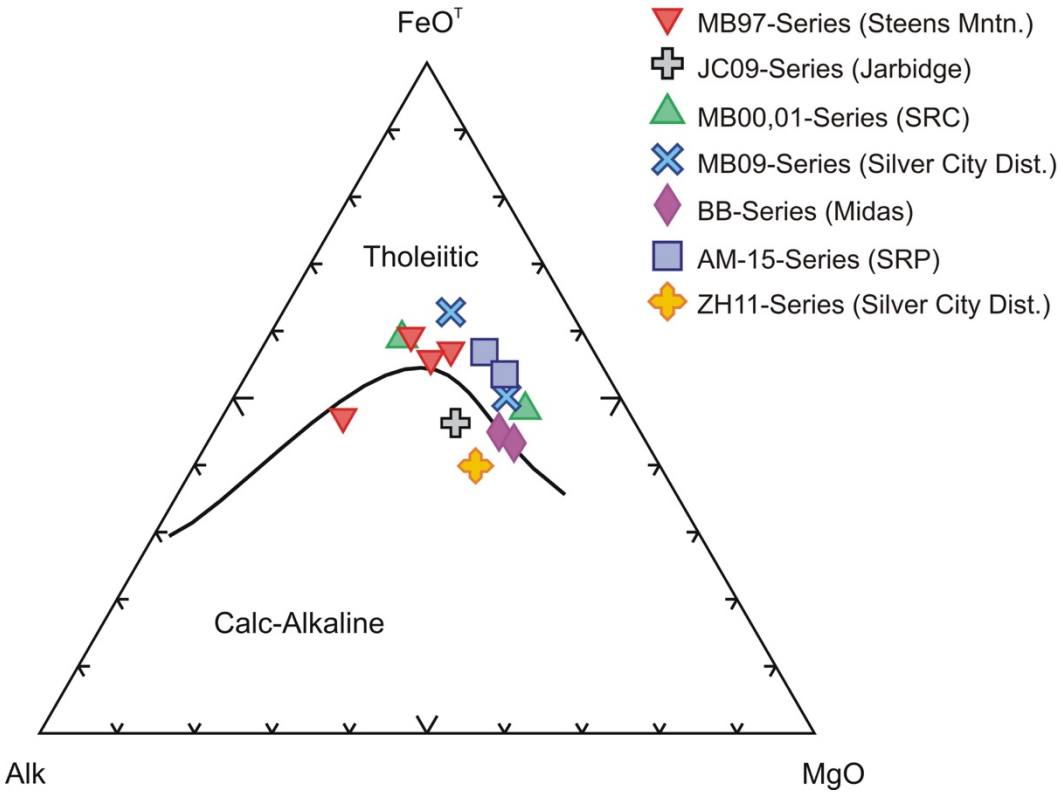

Figure 3-4: AFM diagram (Irvine and Baragar, 1971). Most NGB samples plot as tholeiitic with the exception of three SRC samples that plot just inside the calc-alkaline trend.

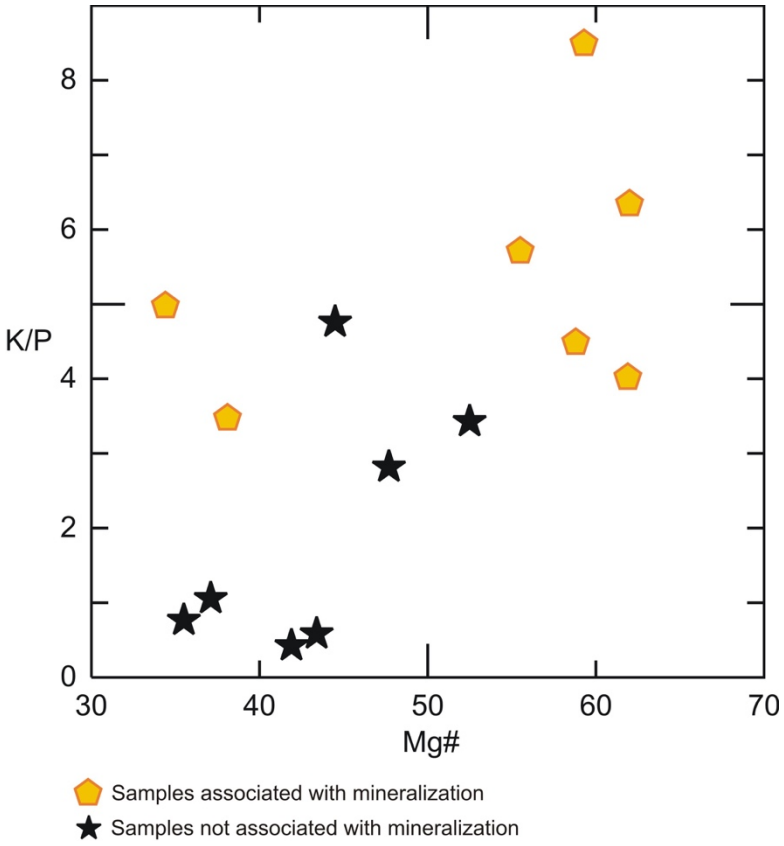

Figure 3-5: K/P ratio vs. Mg#. In general, most NGB samples have a K/P ratio exceeding 3.5, which is consistent with crustal contamination. Most samples known to be associated with mineralization have a higher K/P ratio than those that are not associated with mineralization.

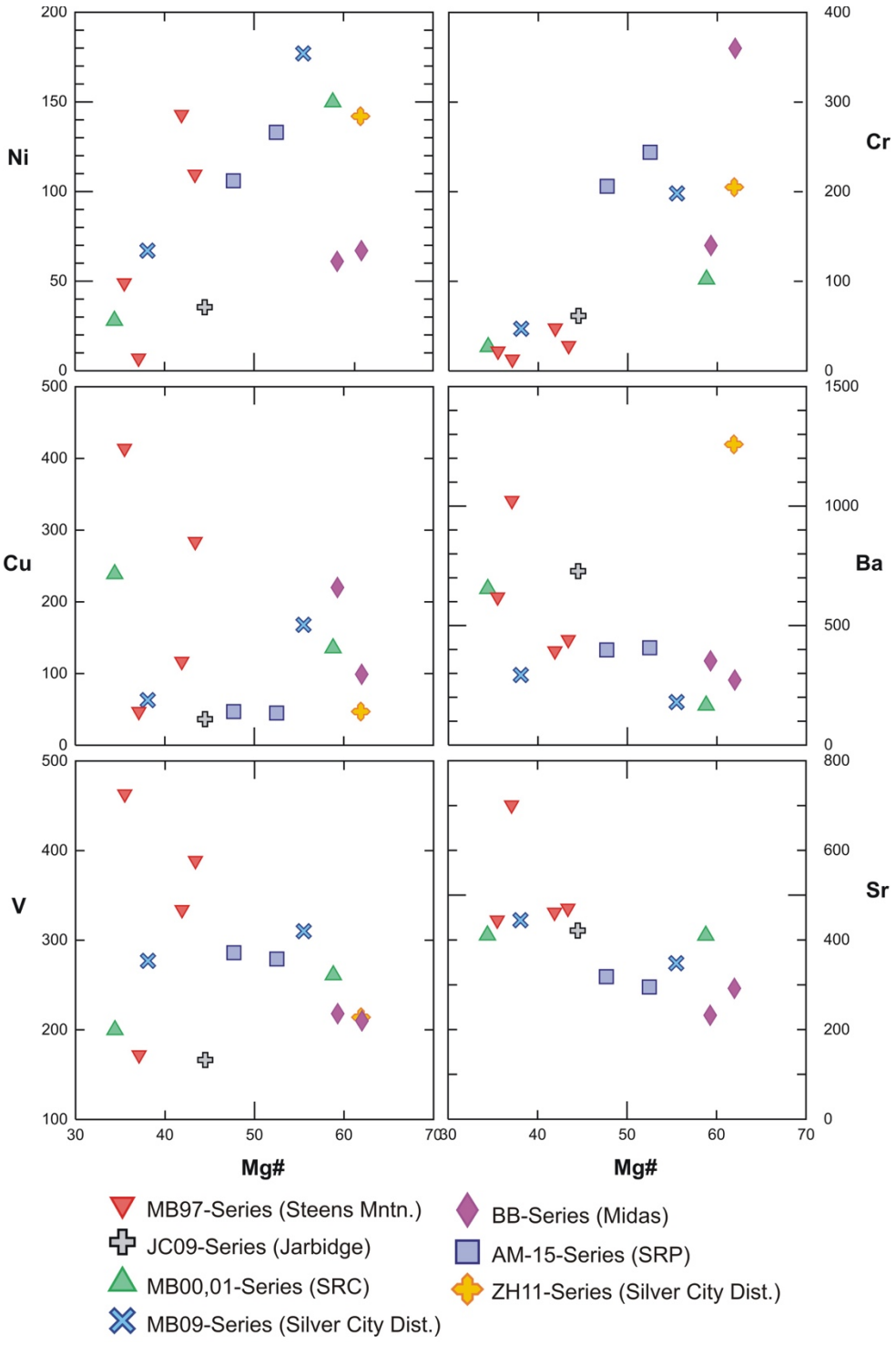

Figure 3-6: Trace elements plotted against Mg#'s. A distinguishable positive correlations exist between Cr and Mg#. A weaker positive correlation can be seen with Ni and a slight negative relationship exists between Sr and Mg#.

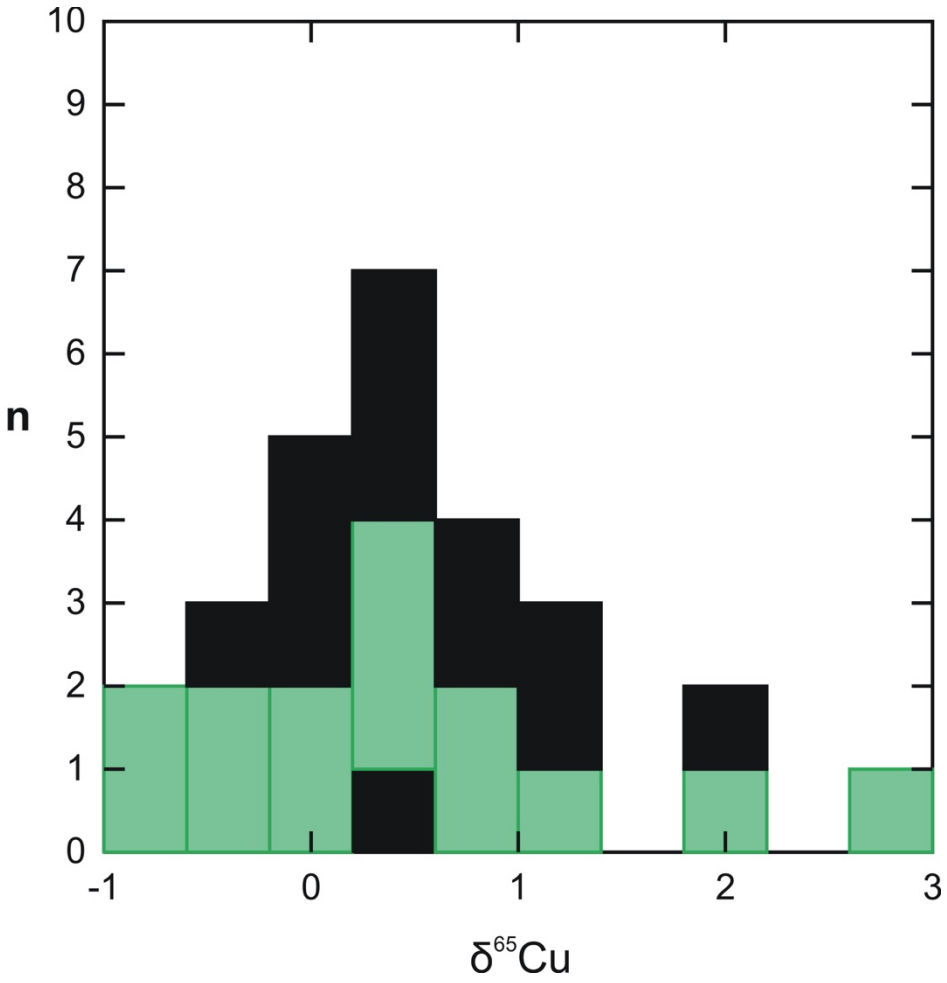

Figure 3-7: Histogram showing NGB samples in green (N= 14) and international standards in black (N= 12). δ^{65}Cu values are reported in ‰. The NGB samples exhibit a larger range of copper isotopic compositions than the standards. Average value for NBG samples and standards together is 0.51‰.

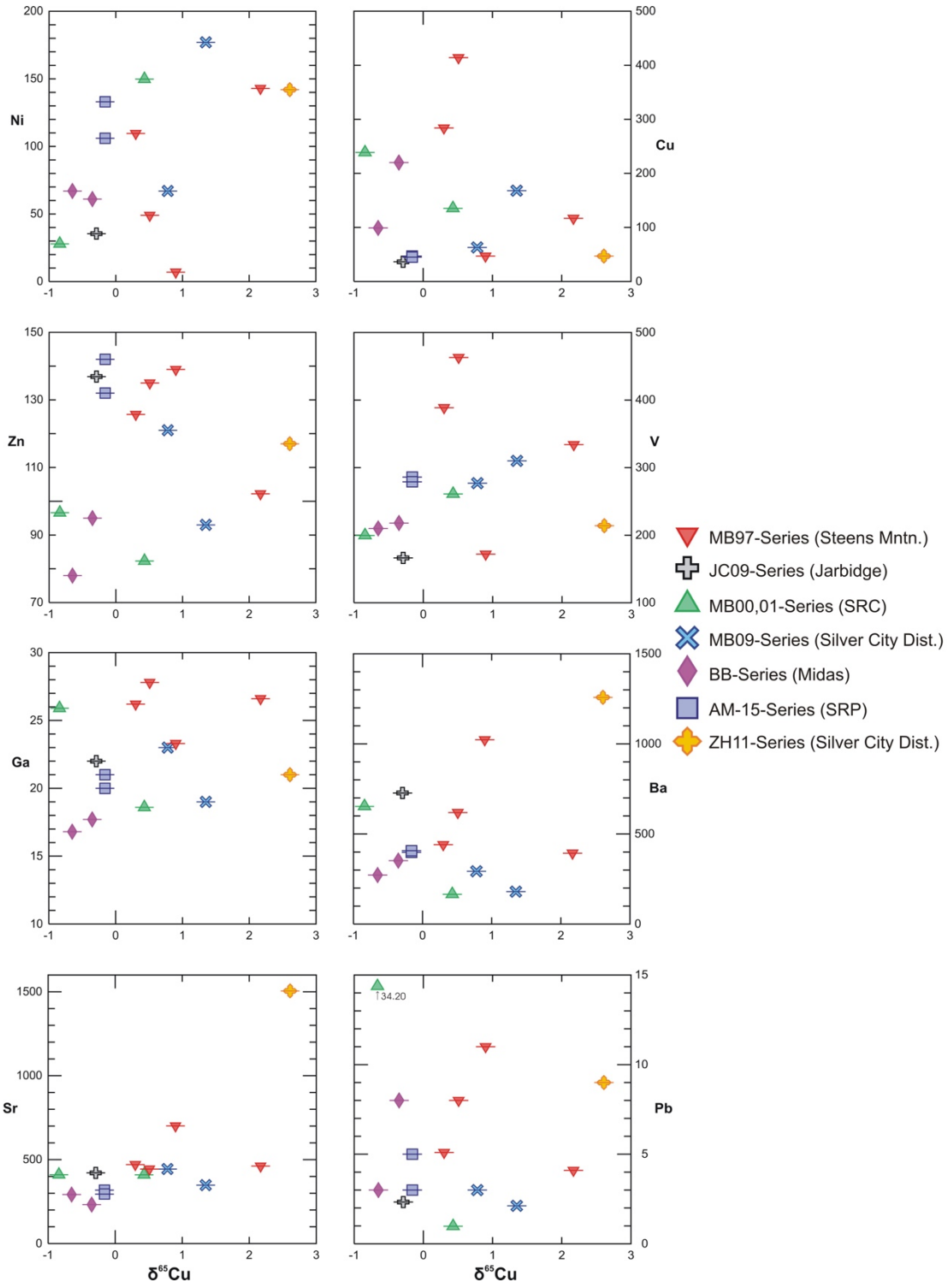

Figure 3-8: Trace elements plotted against Cu isotope composition (‰). Horizontal lines represent 0.14‰ error on all samples. Note the slight positive relationship in Ni, Sr and Ba. Sample associated with mineralization include those from the Jarbidge area, Santa Rosa Calico volcanic field (SRC), and the Silver City district.

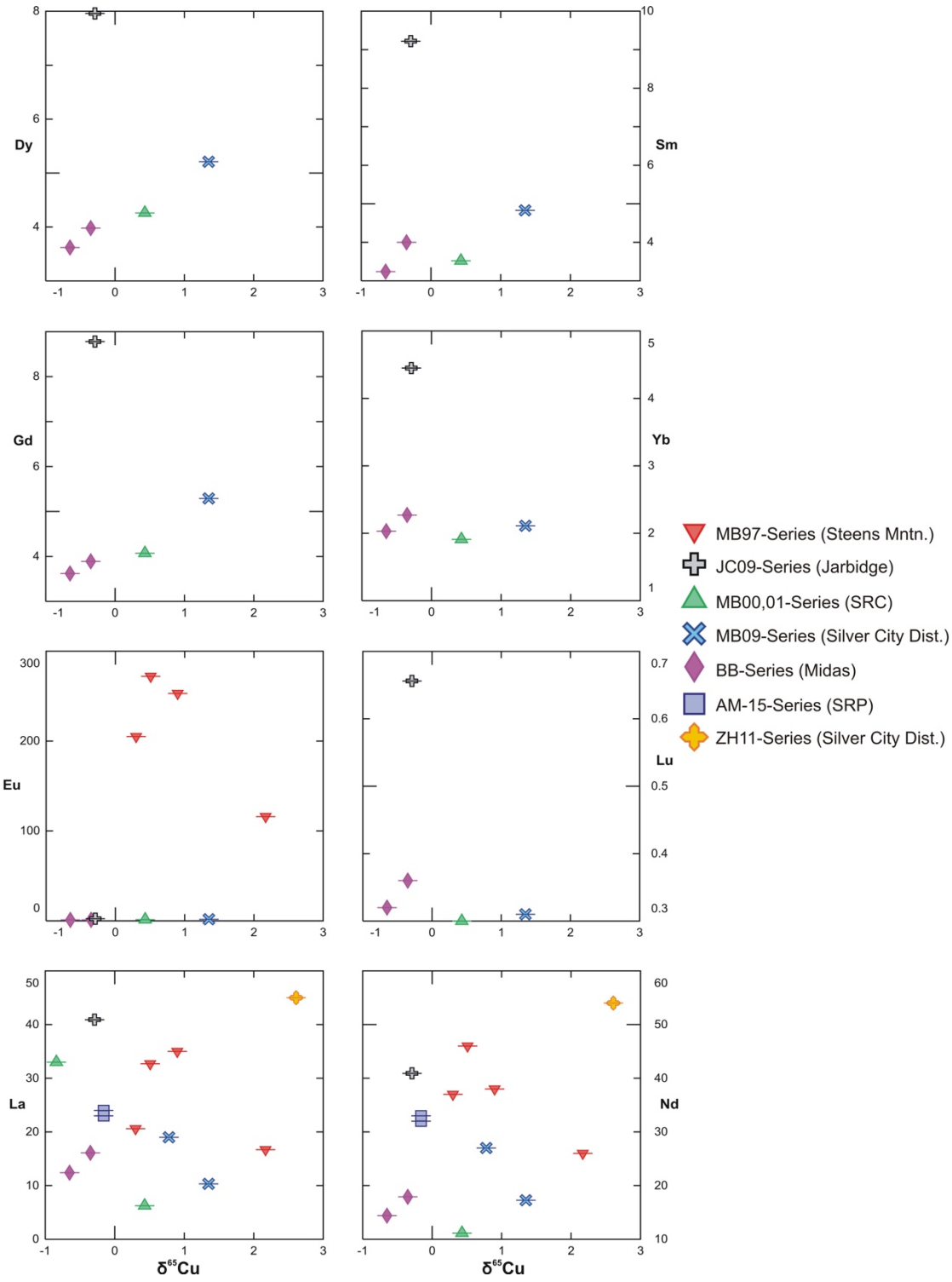

Figure 3-9: Rare earth elements plotted against Cu isotope composition (‰). Horizontal lines represent 0.14‰ error on all samples Note the slight positive relationship in Dy, Sm, and Gd. Samples associated with mineralization include those from the Jarbidge area, Santa Rosa Calico volcanic field (SRC), and the Silver City district.

Chapter 4 - Discussion

Cu Isotope Fractionation Mechanisms and their potential effect on NGB rocks

The limited data that exist regarding $\delta^{65}Cu$ values of mafic rocks suggests that the copper isotopes should be clustered around 0 per mil. The data presented in this study show that mafic rocks/basalts have a much wider range of $\delta^{65}Cu$ values than what has been previously reported (Fig 4-1). Although copper isotope fractionation mechanisms are not well understood, there are several factors known to play a role in this process including redox reactions, crustal contamination and secondary weathering, magma differentiation, mantle melting, vapor-phase transport, and mantle metasomatism.

Redox reactions in hypogene and supergene enrichment zones

Intrusions of dioritic to quartz monzonitic composition are commonly associated with primary processes in porphyry copper deposits (Titley and Beane, 1981; Titley, 1982; Sillitoe, 2010). As these systems are exposed at or near the surface, pyrite and chalcopyrite decompose due to oxidizing fluids and biogenic activity (Titley and Marozas, 1995; Mote et al., 2001; Dold et al., 2009). Copper concentration becomes enriched through chemical reduction of copper and the formation of secondary Cu-sulfide minerals such as chalcocite and covelite (Asadi et al., 2015).

Supergene silicate alteration assemblages are formed from the progressive neutralization of the supergene fluids through hydrogen consumption in reaction with host rocks (Asadi et al., 2015; Graham et al., 2004; Mathur et al., 2005, 2009; Robb, 2005; Maher and Larson, 2007). These reactions typically cause significant copper isotope fractionation at high temperatures greater than 300º C (approximately 0.5‰ fractionation) and/or at low temperatures of less than 50º C (approximately 3‰ fractionation) (Ehrlich et al., 2004; Markl et al., 2006; Asael et al., 2007; Mathur et al 2009, 2010; Asadi et al., 2015). Differences observed in Cu isotopes between the leached cap minerals, hypogene minerals, and supergene enrichment minerals observed in porphyry copper deposits are likely caused by the oxidation of hypogene sulfides and effective trapping of copper in the supergene enrichment zone (Asadi et al., 2015).

The rocks in this study, however, do not appear to contain a significant amount of copper sulfide minerals, which should be present if these reactions took place. This also would not be a

viable hypothesis to explain the fractionation of copper isotopes observed in those continental basalts not related to mineralization.

Low temperature alteration

A few studies have been performed which outline the effects of low temperature alteration (here defined as <300º C) on fractionation in Cu isotopes, particularly in copper porphyry deposits (Seo et al., 2007; Mathur et al., 2009). In this study we do not see enough mineralogical evidence to conclude that low temperature processes are significantly contributing to fractionation. The glass in the matrix for many of these rocks is unaltered, suggesting that little to no alteration occurred after crystallization (Fig. 4-2). Two samples, however, do exhibit some low temperature alteration products such as chlorite (Fig. 4-3). Despite the differences in alteration of these samples, the δ^{65}Cu values do not indicate that low temperature alteration has any effect on Cu isotopic fractionation (Fig 4-4).

Upper crustal contamination

The K/P ratio is used as an indicator of crustal contamination. Ratios of mantle-derived magma, which are uncontaminated, will not exceed 3.5 (Basaltic Volcanism Study Project, 1981; Callicoat, 2010). Some of the Cenozoic rocks described in this study seem to have undergone upper crustal contamination based on their K/P ratios (Fig 3-5). As demonstrated in Figure (4-5) no correlation exists (r^2 = 0.16) between the K/P ratios and δ^{65}Cu values in these rocks suggesting that upper crustal contamination has little to no effect on the fractionation of Cu isotopes. Furthermore, a study by Li et al. (2009) which analyzed the Cu isotope signatures of both I- and S-type granites in SE Australia, proposed that the Cu isotopic composition of the upper continental crust is 0.01 ± 0.30‰ The same study found a 2‰ variation in Cu isotope ratios of granites and some I-type granites had δ^{65}Cu values greater than 1. Thus, the exact effects of upper crustal contamination on Cu isotope fractionation remain inconclusive.

Chemical weathering (CIA & MIA)

Secondary weathering processes, as estimated measured using the CIA and MIA also do not significantly fractionate Cu isotopes in the rocks studied here. Most igneous rocks will have a CIA value between 35 and 50, mafic rocks tending to be on the lower end of this spectrum

(Babechuk et al., 2014). During chemical weathering processes the values of the weathering index will increase due to the loss of mobile elements relative to immobile elements (Babechuk et al., 2014). The average CIA value for the NGB rocks in this study is 44.9, which suggests that these rocks have undergone some chemical weathering. The weathering trend for basalts is typically depicted on an A-CN-K diagram, and is expected to fall along the A-CN join (Nesbit and Wilson, 1992; Babechuk et al., 2014). As seen in Figure (4-6), the values cluster along the A-CN join but do not show any distinguishable trend. Additionally, no correlation exists when the CIA values are plotted against δ^{65}Cu values (Fig.4-7).

The MIA, similar to the CIA is used to analyze the extent of chemical weathering but goes further to include the mafic elements Mg and Fe. Mafic minerals such as pyroxene and olivine are susceptible to chemical weathering and, as a result, Mg is lost from the weathering profile. The weathering of Fe, on the other hand, is redox dependent and differs in reducing environments versus oxidizing environments; thus, two different equations are used to determine the MIA depending on the conditions (Equations 5 & 6). The rocks used for this study are tend to be in oxidizing environments so equation 7 was used to determine the MIA for all NGB samples. Similar to the CIA, as the MIA values increase, so does the extent of weathering. An MIA value of 100 indicates that all of the mobile elements have been removed. The NGB samples in this study have an average $MIA_{(O)}$ value of 38.2. As seen in Figure 4-8 the MIA values increase as Ca, Na, K, and Mg are lost. Likewise, MIA values increase with decreasing concentrations of Mg (Fig. 4-9). Again, this suggests that these rocks have undergone some chemical alteration. However, when MIA values are plotted against δ^{65}Cu values, no relationship is seen (Fig 4-10). Although the exact link between the CIA and MIA and Cu isotope fractionation cannot be determined in this study, it is apparent that chemical weathering processes do not significantly fractionate Cu isotopes.

Mantle partial melting

Copper is a moderately incompatible element and tends to be more enriched in basaltic magmas than the mantle source (Liu et al., 2015). MORBs, OIBs, arc basalts, and primitive basaltic melts tend to have a bulk partition coefficient D_{Cu} mantle/melt of approximately 0.20 – 0.30 (Fellows and Canil, 2012). According to Fellows and Canil (2012) and Lee et al. (2012), the degree of Cu enrichment depends on the modal proportion of sulfides present in the mantle

source, the melt/sulfide ratio, and the oxidation state of the mantle. Liu et al. (2015) found that the degree of mantle melting in metasomatized peridotites and non-metasomatized peridotites may help explain the fractionation observed in Cu isotopes. The degrees of partial melting, however are not equal in all types of basalts. or example OIBs are typically generated by lower degrees of melting (~5%) (McKenzie and O'Nions, 1995), MORBs by moderate degrees of melting (10-15%) (Klein and Karsten, 1995), and arc basalts by high degrees of melting (10-25%) (Plank and Langmuir, 1998). Since sulfide is a residual phase until about 25% melting in fertile mantle (Hamlyn et al., 1985) some Cu will be left behind in the mantle, especially MORBs and OIBs (Liu et al., 2015), which may lead to isotope fractionation.

The NGB basalts analyzed in this study exhibit a large isotopic variation as do arc basalts and continental basalts (Table 1-1), MORBs and OIBs (Liu et al., 2015) on the other hand exhibit a relatively homogenous Cu isotopic composition (Table 1-1). If mantle melting were the contributing factor for Cu isotope fractionation, one would expect to see a unidirectional shift in the isotope compositions (Liu et al., 2015). This is not the case. Therefore, magma differentiation due to mantle melting cannot be used to explain the range in Cu isotopes that we see in this study.

Mantle metasomatism

During lithospheric thinning, melting occurs and magmas tend to "pond-up" at the bottom of the lithosphere or crust/mantle boundary. As these magmas ascend, they begin to crystallize and may interact with the products of previous episodes of magmatism, particularly during continued extension. This sequence of magmatism, crystallization, and eventual volcanism creates a repetitive process that may be significantly contributing to Cu isotopic fractionation.

In subduction zones, Cu is considered to be a highly fluid-mobile element especially during slab dehydration, which plays an important role in the transport of Cu from subduction zones into the mantle wedge (Liu et al., 2015). Since the primary hosts of porphyry copper deposits are magmas generated in the arc mantle wedge, by understanding the transport of copper from the subducting slab to the arc wedge we can gain a better understanding of porphyry copper deposits (Liu et al., 2105) and possibly other high grade ore deposits which are generated from metals in the mantle. The mechanisms of Cu enrichment in copper porphyry deposits are

still being debated. Mungall (2002) proposed that either the subducting slab or arc mantle contains an anomalously copper-rich source due to the sulfide breakdown in oxidizing conditions. Lee et al. (2012) on the other hand proposed that magmatic differentiation processes in the crust enhance copper enrichment with little contribution from the mantle or subducting slab.

In samples analyzed across the Kamchatka arc (Liu et al., 2015) the heaviest δ^{65}Cu values are located farthest away from the trench and the lightest values are located closer to the trench. The two mechanisms proposed by Liu et al. (2015) to explain this observation are 1) isotopic heterogeneity of the source and slab fluids, or 2) different degrees of partial melting. As discussed above, partial melting does not adequately explain the large range of Cu isotope values seen for arc, continental basalts, and NGB basalts. It is more likely that slab fluids involved in melting during slab dehydration result in heterogeneity of the mantle source and the variation in δ^{65}Cu values is a signature from that source. Although data regarding Cu isotopic compositions in sedimentary rocks are limited, oceanic sediments tend to show slightly positive values. For example, Cu associated with Fe-Mn nodules is characterized by a δ^{65}Cu value of 0.31 ± 0.23‰, Albarede (2004). Dekov et al. (2013) found that δ^{65}Cu values in oceanic sedimentary layers ranged from 0.41 to 0.95‰. The Cu value in seawater itself shows positive values between 0.8 and 1.5‰ (Vance et al., 2008; Takano et al., 2013; Thompson et al., 2013).

Vapor phase transport

In previous studies it was thought that the agent of metal transport in the genesis of hydrothermal ore deposits was in an aqueous liquid even though several studies had reported higher concentrations of Cu in the vapor phase from porphyry-type deposits (Damman et al., 1996; Heinrich et al., 1999; Ulrich et al., 1999; Baker et al., 2004). However, more recent work (e.g., Heinrich et al., 2004; Williams-Jones and Heinrich 2005; Saunders et al., 2015) suggests that volatile metals and metalloids, along with sulfur are transported to epithermal environments in low-density magmatic "vapors." This vapor-phase transport of ore metals may be instrumental in the emplacement of high-grade epithermal ore deposits. Not only can this process lead to significant fractionation of metals and selective enrichment of ore-forming components (Williams-Jones and Heinrich, 2005) but it has also been suggested that this may lead to significant fractionation of isotopes, such as Cu (Saunders et al., 2015).

^{65}Cu is two neutrons heavier than ^{63}Cu and more energy is required to vaporize the heavier isotope. This likely enriches the vapor in ^{63}Cu leaving the liquid left behind enriched in ^{65}Cu. As the ^{63}Cu rich-vapor is transported and becomes incorporated into the surrounding rocks, it can be measured as a more negative isotopic ratio, whereas the ^{65}Cu-rich liquid would have a more positive signature. Because the ores are forming from the volatiles released by magmatic intrusions, the vapor phase should become incorporated in the ore minerals, thus creating a more negative isotopic ratio. This does not explain, however, why we see such a broad range in the Cu isotopes, especially in ore deposits such as Au-Ag epithermal and porphyry Cu deposits. Due to the limited data obtained in this study and the limited knowledge of vapor-phase transitions, it cannot be conclusively stated that vapor phase transport does or does not contribute to Cu isotope fractionation.

Cu Isotope compositions of NGB/SRP magmas and coeval epithermal deposits

The $\delta^{65}Cu$ values of ore minerals from Buckskin National, Sleeper, Jumbo, Midas, Ivanhoe, War Eagle Mountain, DeLamar Mtn., and Trade Dollar Mines range from -2.70 to +3.25‰ and have an average of 0.24‰ (Saunders et al., 2015). This is a larger range compared with the $\delta^{65}Cu$ values seen in the NGB rocks (-0.84 to +2.61‰), which have an average of 0.47‰. However, as shown in Figure 4-1 the majority of the values from the ores, the NGB rocks, metallic meteorites, and mantle rocks overlap. As recent studies have suggested (Saunders et al., 2008; Williams-Jones and Heinrich, 2005; Saunders et al., 2015), elements in ore minerals, especially those found in porphyry copper deposits and epithermal Au-Ag deposits ultimately are sourced from the mantle. The Cu isotope data presented in this study verifies that the ore metals in NGB epithermal deposits are coming from a magmatic source, the same source from which the basalts originated. Based on these findings, I suggest that the Cu isotopic composition in the mantle source may in fact be heterogeneous and the range in $\delta^{65}Cu$ values seen in both the ores and the basalts reflect this source signature.

Comparisons of Cu isotopes in NBG rocks, international standards, and rocks from previous studies

The variation in Cu isotopic compositions of NGB rocks (-0.84 to +2.61‰) and international standards (-0.43 to +2.00‰) observed in this study greatly expands the known

range of Cu isotope data, not only for basalts but also for andesites, and peridotites, as well. This larger range may indicate that the Cu isotope composition of the mantle is not 0‰ as previously thought, and suggests that the mantle is likely heterogeneous. The Cu isotope data presented here also overlaps with reported values from regional bonanza (Au-Ag) epithermal ores (-2.5 to +3.5‰) (Saunders et al., 2015). Porphyry copper deposits have a much broader range of Cu isotopic compositions (-13.5 to +8.31‰) and show a distinct separation of δ^{65}Cu values, where the leach cap minerals<hypogene minerals<supergene enrichment minerals (e.g., δ^{65}Cu values from leach cap minerals, hypogene minerals, and supergene minerals of the Silver Bell deposit were reported by Mathur et al. [2012] respectively; -8.43, -2.63, and 4.85‰). The difference in ranges of Cu isotope values between the different types of ore deposits may reflect a signature that results from ore genesis processes. By understanding the mechanisms of Cu fractionation it may be possible to use δ^{65}Cu values as an effective exploration tool.

Although this work greatly expands the known range of Cu isotope data, it is unclear which dissolution method would be ideal in analyzing samples in the future. My results show different values for the international rock standards than what has been previously analyzed (Table 4-1). These previous studies used the whole rock dissolution method to analyze samples, whereas in this study, samples were leached using aquaregia. Previous studies examining the copper isotopic compositions of ore minerals (e.g., Mathur et al., 2012; Saunders et al., 2015) used the leaching method as well. Future work will aim to shed some light on which dissolution method would be preferable by determining the host phase that the copper is in (Zweifelhofer, per. comm.).

Table 4-1: Cu isotopic compositions of igneous rock standards reported in this study and previous works.

Sample	Reference	δ^{65}Cu Value (‰)	Dissolution method used
BHVO-2	Liu et al. (2015)	0.13 ± 0.05	Whole rock dissolution
	Liu et al. (2014)	0.15 ± 0.05	Whole rock dissolution
	This study	**0.43 ± 0.14**	**Aquaregia leach**
	Moeller et al. (2012)	0.10 ± 0.04	Whole rock dissolution
BCR-2	Liu et al. (2015)	0.21 ± 0.05	Whole rock dissolution
	Liu et al. (2014)	0.22 ± 0.04	Whole rock dissolution
	This study	**2.00 ± 0.14**	**Aquaregia leach**
	Bigalke et al. (2010)	0.19 ± 0.08	Whole rock dissolution
	Moeller et al. (2012)	0.14 ± 0.05	Whole rock dissolution
BCR-1	Archer and Vance (2004)	0.07 ± 0.08	Whole rock dissolution
AGV-2	Liu et al. (2015)	0.06 ± 0.05	Whole rock dissolution
	Liu et al. (2014)	0.05 ± 0.04	Whole rock dissolution
	This study	**0.40 ± 0.14**	**Aquaregia leach**
AGV-1	Moeller et al. (2012)	0.11 ± 0.04	Whole rock dissolution
JB-3	**This study**	**-0.43 ± 0.14**	**Aquaregia leach**
	Liu et al. (2014)	0.16 ± 0.03	Whole rock dissolution

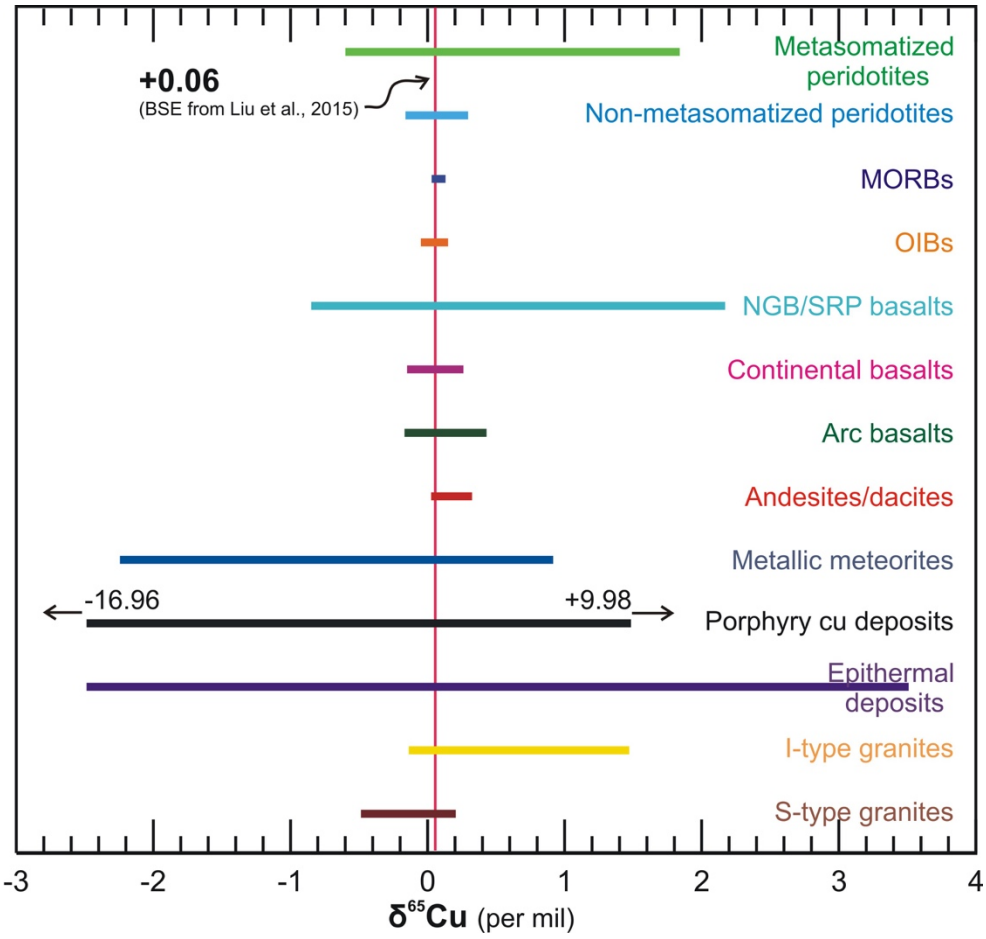

Figure 4-1: The $\delta^{65}Cu$ ranges of various lithologies as reported by previous studies. Data source: peridotites, arc basalts, continental basalts, and andesites/dacites (Liu et al., 2015), MORBs (Ben Othman et al., 2006), OIBs (Ben Othman et al., 2006; Li et al., 2009), NGB/SRP basalts are from this study, I-type and S-type granites from the Lachlan fold belt, southeast Australia (Li et al., 2009), porphyry copper deposits (Mathur et al., 2008, Li et al. (2010) and Asadi et al. (2015), epithermal deposits (Saunders et al., 2015), and metallic meteorites (Luck et al., 2003).

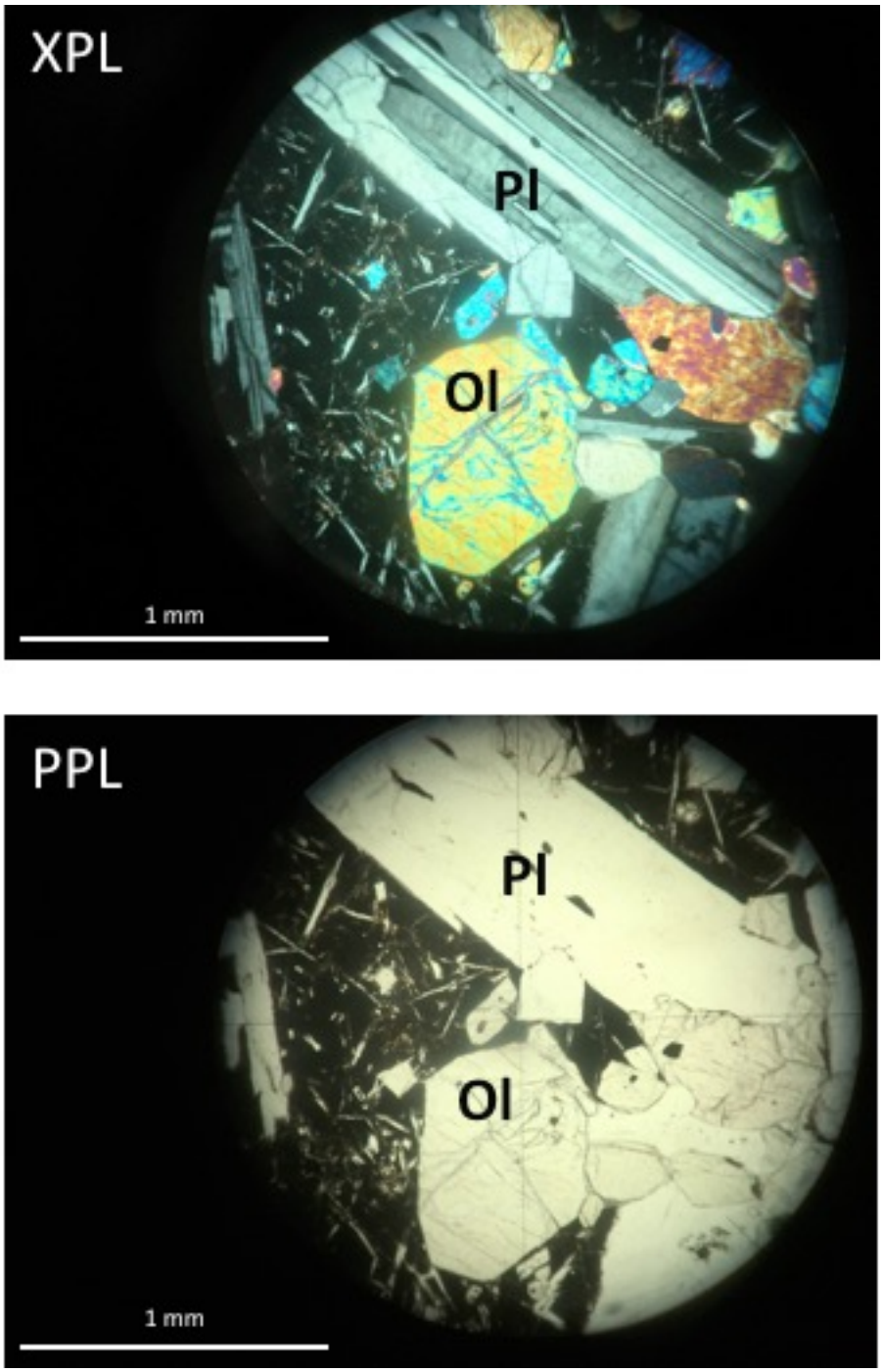

Figure 4-2: Photograph of thin-section from sample AM15-3. The top image is in crossed polarized light (XPL) and the bottom image is in plane polarized light (PPL). Pl represents plagioclase and Ol represents olivine. Notice the unaltered glassy matrix and lack of iddingsite around the olivine grain.

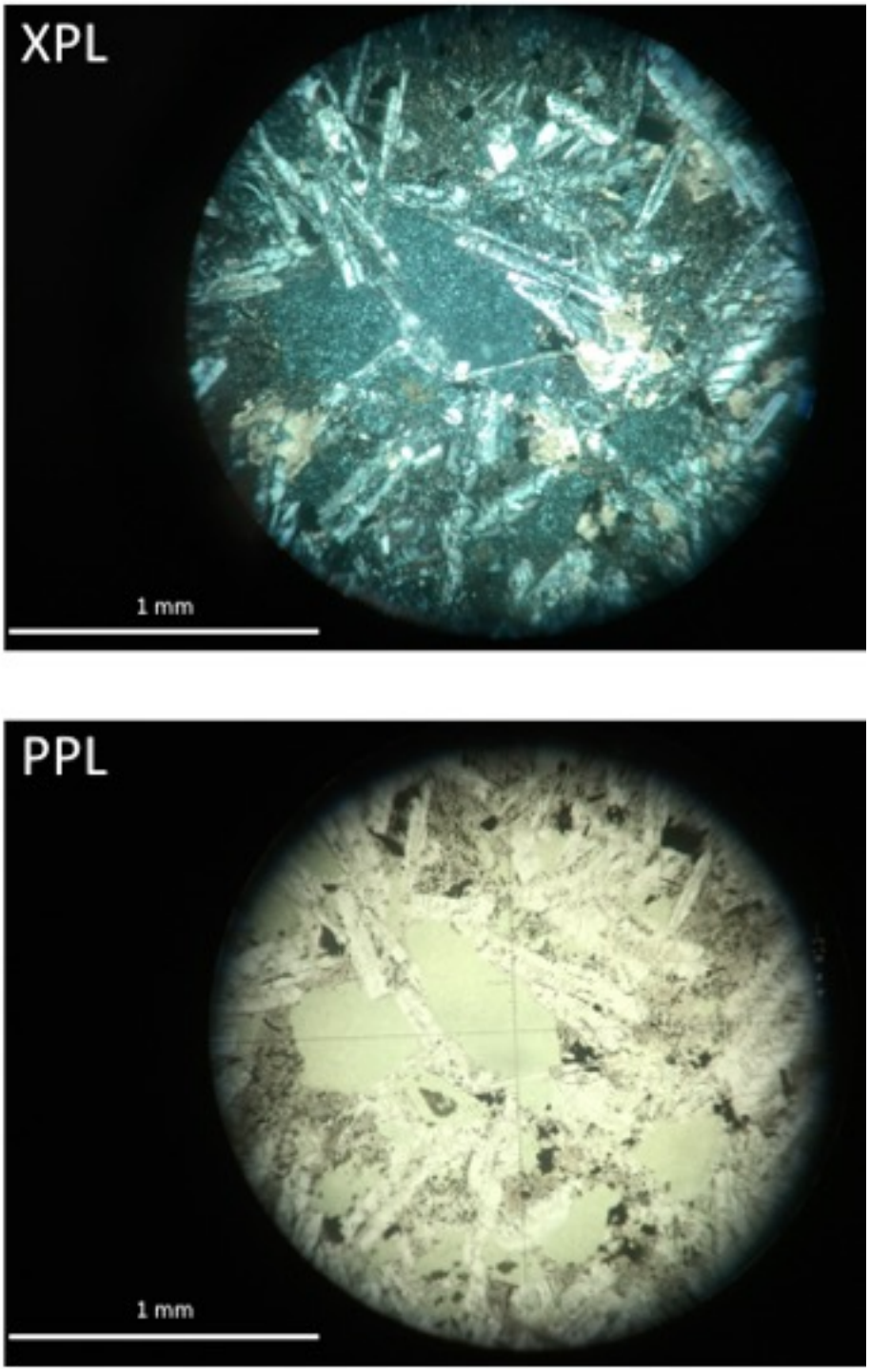

Figure 4-3: Photograph of thin-section from sample 2-12BB. The top image is in crossed polarized light (XPL) and the bottom image is in plane-polarized light (PPL). Notice the extensive low temperature alteration seen here as chlorite (green in PPL and anomalous green/blue interference colors in XPL).

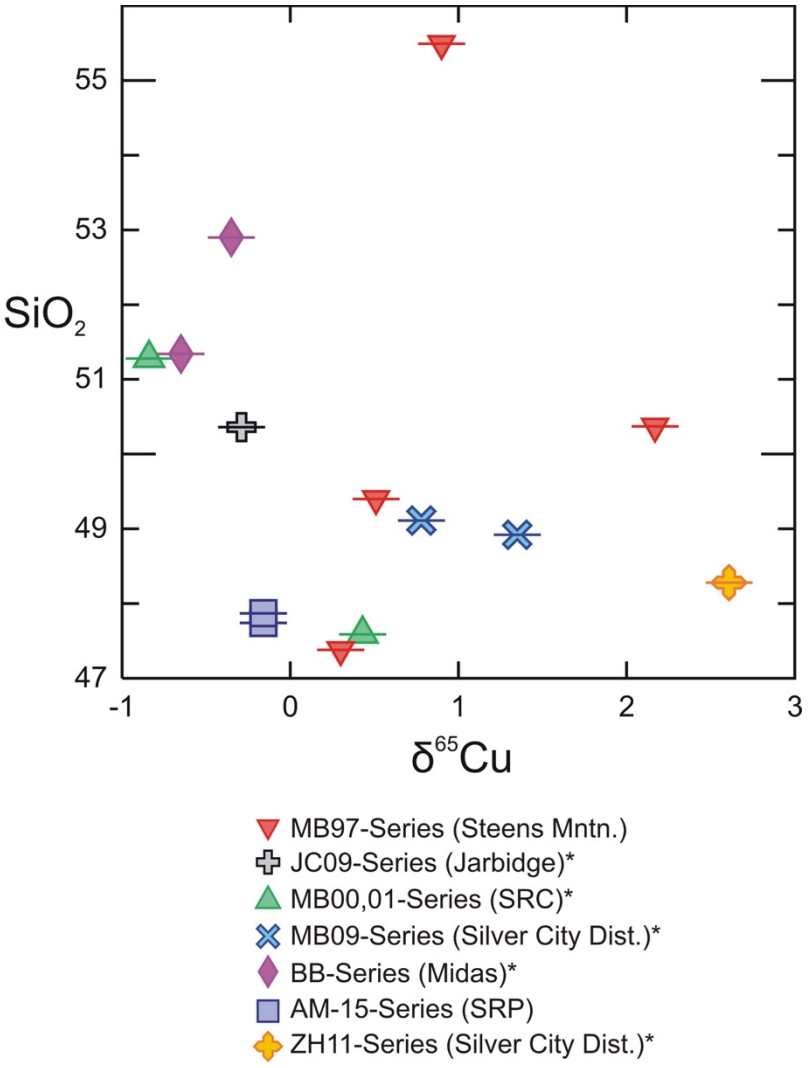

Figure 4-4: Graph of $\delta^{65}Cu$ (‰) vs. SiO_2. Horizontal lines represent 0.14‰ error on all samples. Notice the close proximity of the BB samples (pink diamonds) and the AM samples (blue squares). The Cu isotope compositions of these four samples are very similar despite differences in low temperature alteration.

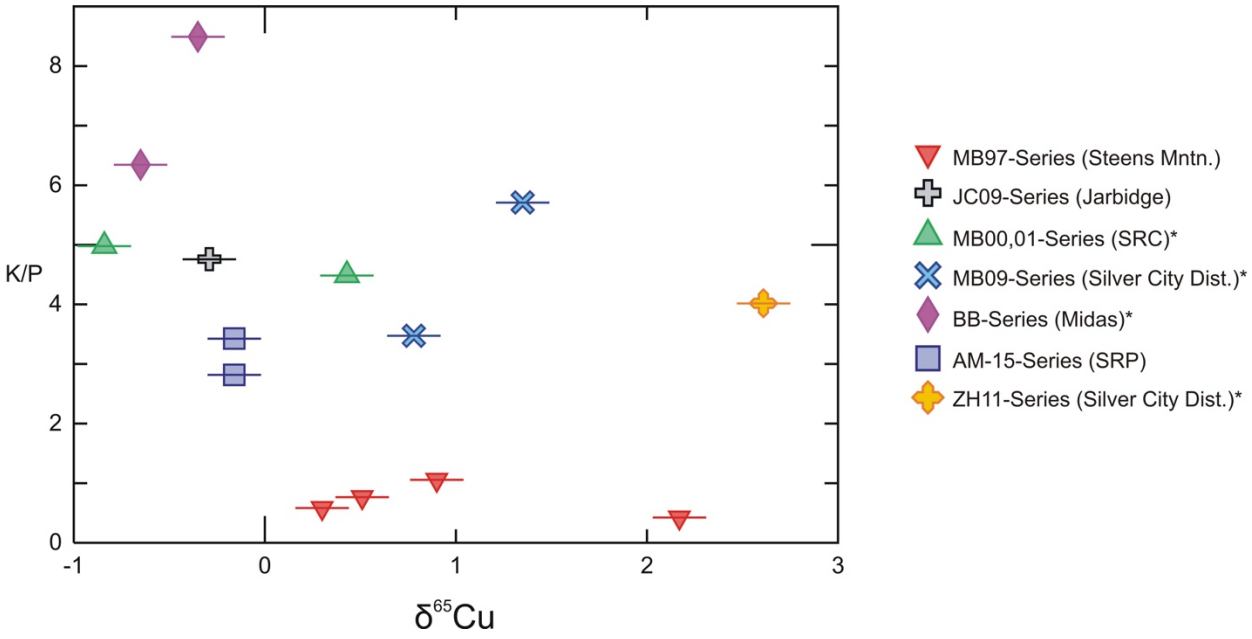

Figure 4-5: K/P ratio plotted against δ^{65}Cu isotope composition. Horizontal lines represent 0.14‰ error on all samples. Notice that most samples exhibit a high K/P ratio consistent with crustal contamination. No distinguishable relationship exists; thus crustal contamination must not be the contributing factor for Cu isotope fractionation

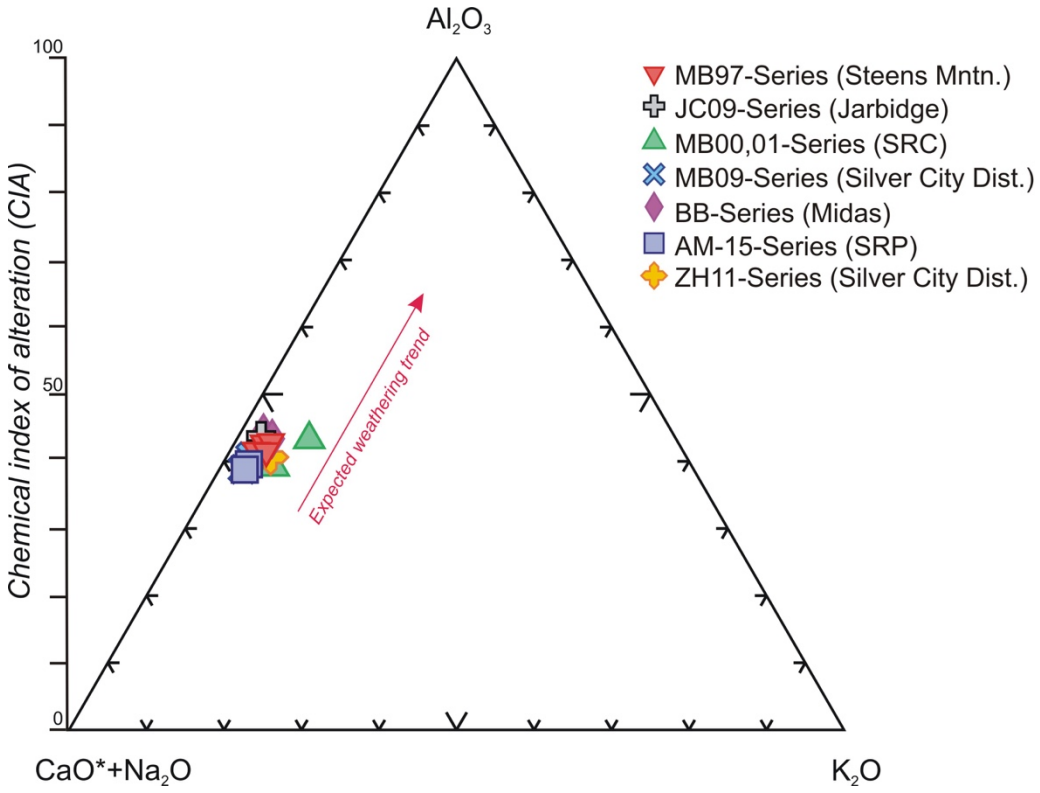

Figure 4-6: A-CN-K plot with the CIA denoted on the left hand side. Notice how all values cluster along the A-CN join just below a CIA value of 50.

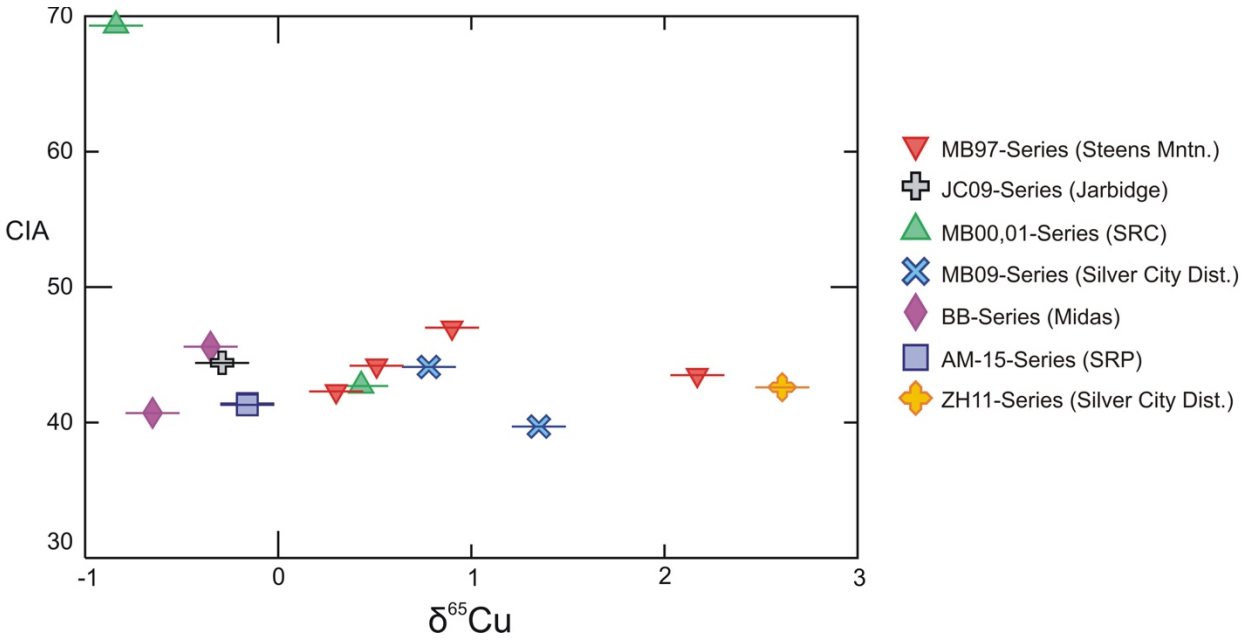

Figure 4-7: CIA vs. δ^{65}Cu (‰) isotopic composition. Horizontal lines represent 0.14‰ error on all samples. No discernable relationship exists suggesting that chemical weathering does not contribute to copper isotope fractionation.

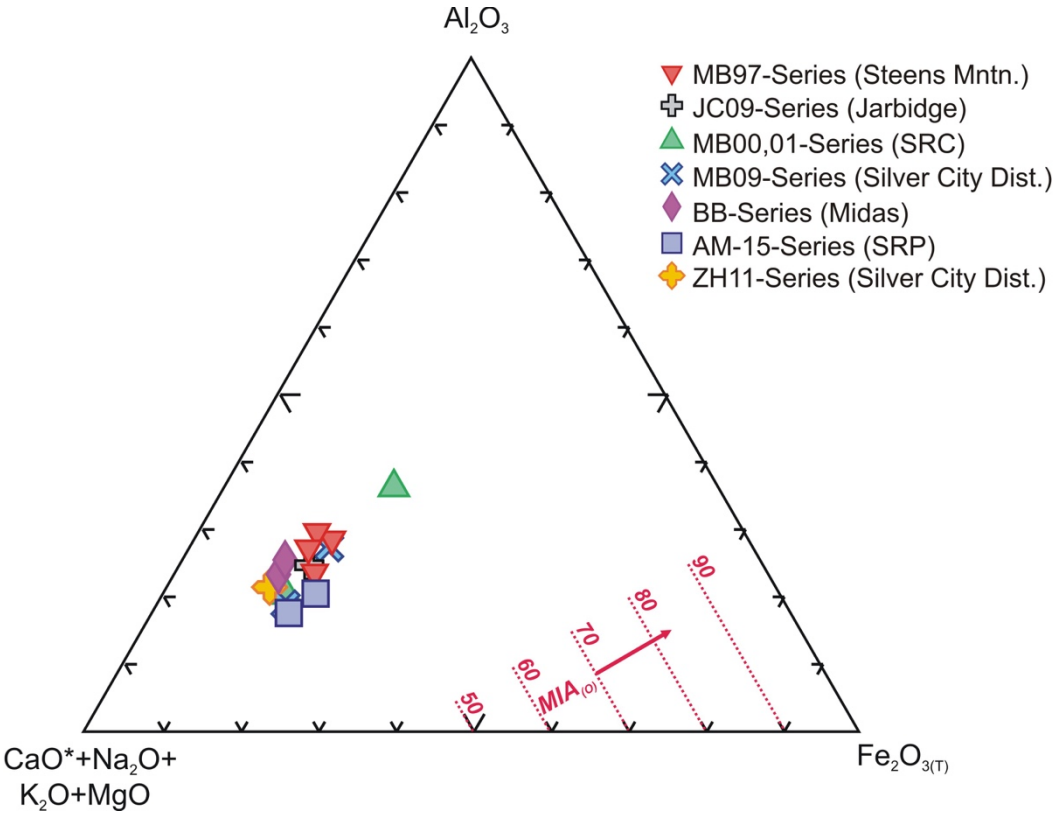

Figure 4-8: Molar ternary plot in A-CNKM-F space with MIA(O) increasing toward the the A-F join. Samples mainly cluster below an MIA(O) of 50 and do not display any particular weathering trend.

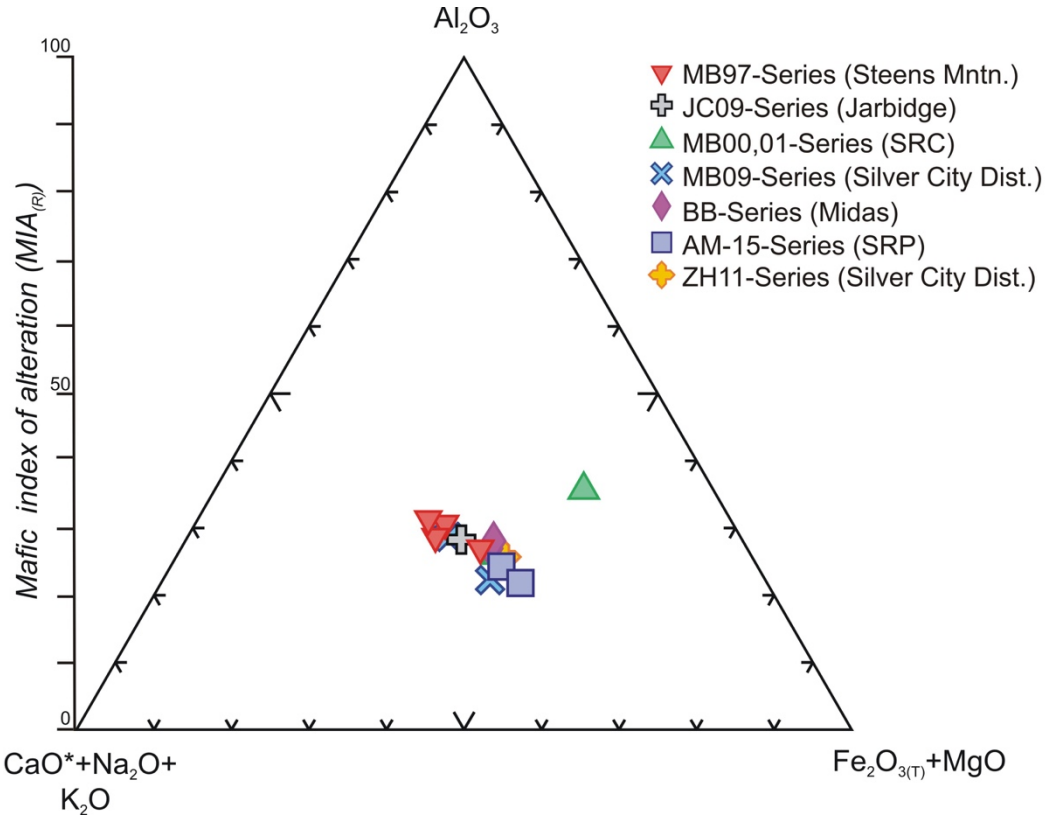

Figure 4-9: Molar ternary plot in A-CNK-FM space with $MIA_{(R)}$ increasing toward the Al_2O_3 point of the plot. Samples do not display any particular weathering trend.

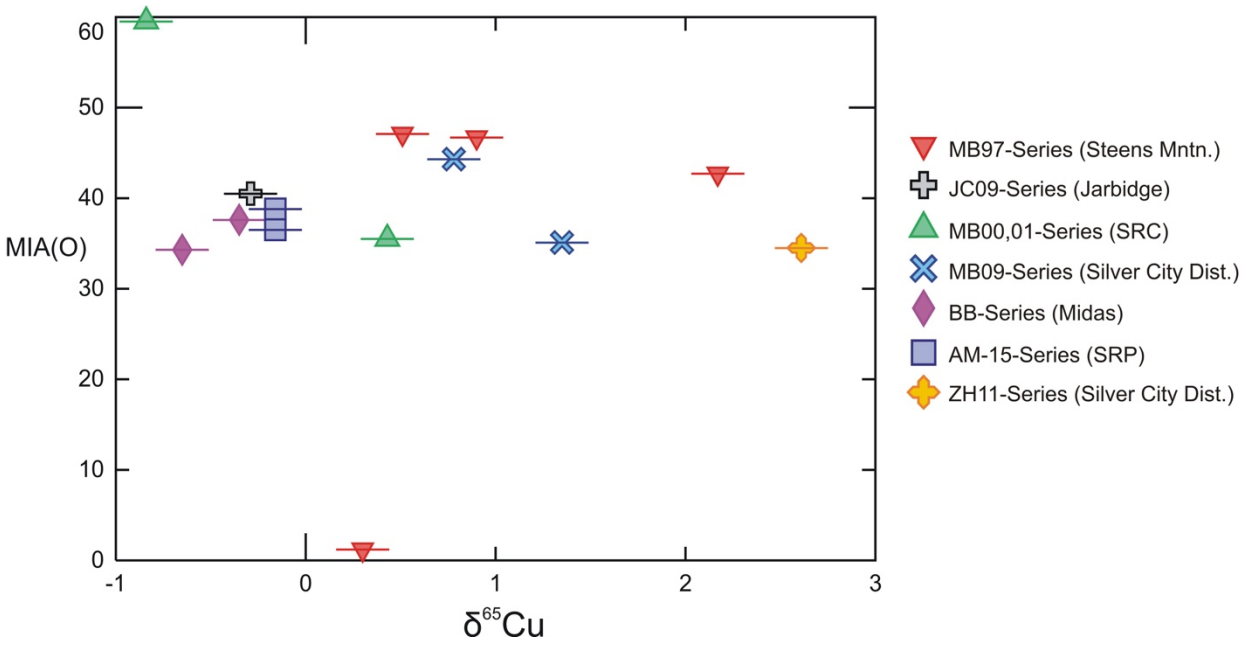

Figure 4-10: MIA vs. δ^{65}Cu (‰) isotope composition. Horizontal lines represent 0.14‰ error on all samples No relationship exists, suggesting that secondary weathering processes do not significantly contribute to Cu isotope fractionation processes.

Chapter 5 - Conclusions

(1) The range in Cu isotopic composition of the 14 NGB/SRP mafic rocks analyzed in this study is -0.84 to +2.17‰, with an average of +0.51‰.

(2) The 12 ultramafic to mafic international rock standards analyzed show a range in Cu isotopic composition of -0.43 to +2.00‰ with an average of 0.47‰

(3) Cu isotope compositions of NGB basalts overlap extensively with regional ores and mantle rocks, which verifies a deep magmatic source for the ores.

(4) This work greatly expands the known range of Cu isotopes not only for basalts but for peridotites, and andesites as well. The large range observed is possibly due to heterogeneity in the mantle, which does not support previous hypothesis regarding mantle homogeneity with respect to Cu isotope composition.

(5) Although it is still unclear what exact processes cause the fractionation of Cu isotopes, it is likely that either liquid-vapor transitions or mantle metasomatism, or both play a critical role.

Chapter 6 - Suggested Future Work

Cu isotopes can be used as a geochemical exploration tool that may be critical in the investigation of future ore deposits. Analyzing the δ^{65}Cu values in both minerals and whole rocks will help broaden our understanding of ore deposits such as porphyry copper and epithermal Au-Ag deposits. The Northern Great Basin (USA), which is host to many high-grade epithermal deposits, is a prime region to investigate the links between Cu isotope fractionation and ore genesis. There are still questions that need to be addressed before a definitive conclusion can be made regarding fractionation mechanisms.

(1) Using a reflected light microscope on a few of the samples in this study indicated that sulfides are not in abundance in these rocks. Typically, copper will form sulfides (usually with iron) but can also be contained in magnetite or glass. As suggested by Eldholm (1989), copper also partitions into feldspars, such as plagioclase, and Cu-rich feldspars are present in mid-Miocene Steens basalt lavas where in some cases it actually exsolves into native Cu inclusions (e.g., "Oregon Sunstones"; Hofmeister and Rossman, 1985). It would be helpful to know where the copper is partitioning into in these rocks. The most efficient way of answering this question would likely involve microprobe elemental mapping.

(2) Although this study greatly expands the range of δ^{65}Cu values for basalts the database as a whole is still limited. More studies with numerous samples of not only basalts but other lithologies will greatly improve our knowledge of Cu isotope fractionation.

(3) More work needs to be done in regions where mantle xenoliths can be analyzed along with basalts that are intrinsically linked to those xenoliths; this may give more insight into mantle heterogeneity.

(4) This work was unable to reproduce standard values measured by workers in previous studies, thus other dissolution techniques such as whole rock dissolution should be explored.

References

Albarede, F., (2004) The Stable Isotope Geochemistry of Copper and Zinc. Reviews in Mineralogy and Geochemistry, Vol. 55, pp. 409-427.

Archer, C., Vance, D., 2004. Mass discrimination correction in multiple-collector plasma source mass spectrometry: an example using Cu and Zn isotopes. J. Anal. At. Spectrom. 19, 656–665.

Armstrong, R. L., Leeman, W. P., and Malde, H. E., 1975, K–Ar dating Quater- nary and Neogene volcanic rocks of the Snake River Plain, Idaho: American Journal of Science, v. 275:3, p. 225–251.

Asadi, S., Mathur, R., Moore, F., Zarasvandi, A., 2015, Copper isotope fractionation in the Meiduk porphyry copper deposit, Northwest of Kerman Cenozoic magmatic arc, Iran. Terra Nova, doi: 10.1111/ter.12128

Asael, D., Mathews, A., Bar-Mathews, M. and Halicz, L., 2007. Copper isotope fractionation in sedimentary copper mineralization (Tima Valley, Israel). Chem. Geol., 243, 238–254.

Babechuk, M.G., Widdowson, M., Kamber, B.S., 2014, Quantifying chemical weathering intensity and trace element release from two contrasting basalt profiles, Deccan Traps, India. Chemical Geology, Vol. 363, pp. 56-75

Baker, T., Van Achterberg, E., Ryan, C.G, and Lang, J.R., 2004, Composition and evolution of ore fluids in a magmatic-hydrothermal skarn deposit: Ge- ology, v. 32, p. 117–120.

Basaltic Volcanism Study Project, Basaltic volcanism on the terrestrial planets. 1286 pp., Pergamon, New York, 1981.

Bigalke, M., Weyer, S., Kobza, J., Wilcke, W., 2010. Stable Cu and Zn isotope ratios as tracers of sources and transport of Cu and Zn in contaminated soil. Geochim. Cosmochim. Acta 74, 6801–6813.

Boyle, E.A., Sclater, F.R., Edmond, J.M, (1997) The distribution of dissolved copper in the Pacific. Earth Planet Sci Lett 37:38-54

"BRGM, THE FRENCH GEOLOGICAL SURVEY." BRGM, Web. 09 Aug. 2016

Bruland, K.W, (1983) Trace elements in seawater. In: Chemical Oceanography. Riley, J.P., Chester, R., (eds) Acad. Press, London, 8:157-220

Bruland, K.W., Franks R.P., (1983) Mn, Ni, Cu, Zn, and Cd in the western North Atlantic. In: Trace Metals in Seawater, NATA Conf Ser. 4 Mar. Chem Geol. Wong CS, Boyle, E.A., Bruland, K.W., Burton, J.D., (eds) Plenum, New York, 9:395-414.

Brueseke, M.E. and Hart, W.K., 2008, Geology and petrology of the mid-Miocene Santa Rosa-Calico volcanic field, northern Nevada. Nevada Bureau of Mines and Geology Bulletin #113

Brueseke ME, Heizler MT, Hart WK, Mertzman SA (2007) Distribution and geochronology of Oregon Plateau (U.S.A.) flood basalt volcanism: the Steens Basalt revisited. J Volcanol Geotherm Res 161:187–214

Brueseke, M.E., 2006, Mid- Mid-Miocene Magmatic System Development in the Northwestern United States, Illinois State University, Department of Geology-Geography.

Brueseke, M.E., 2010, Magmatism and mineralization in the northern Great Basin: mid-Miocene volcanism related to the inception of the Yellowstone hotspot and its relationship to regional bonanza ore deposits, Geological Society of Nevada 2010 Symposium.

Brueseke, M.E., Callicoat, JS., Hames, W., and Larson, PB., 2014, Mid-Miocene rhyolite volcanism in northeastern Nevada: the Jarbidge Rhyolite and its relationship to the Cenozoic evolution of the northern Great Basin (USA): GSA Bulletin., v. 126, p. 1047-1067

Callicoat, J.S., (2010) Significance of Mid-Miocene Volcanism in Northeast Nevada: Petrographic, chemical, Isotopic, and Temporal importance of the Jarbidge Rhyolite. [M.S. thesis] Manhattan, Kansas State University.

Camp, V.E., 1995, Mid-Miocene propagation of the Yellowstone mantle plume head beneath the Columbia River Basalt source region: Geology, v. 23, p. 435–438, doi:10.1130/0091-7613(1995)023<0435:MMPOTY>2.3.CO;2.

Camp, V.E., 2013, Origin of CRB: Passive rise of shallow mantle, or active upwelling of a deep-mantle plume? GSA Spec. Pap. 497, 181-199.

Camp VE, Ross ME (2004) Mantle dynamics and genesis of mafic magmatism in the intermontane Pacific Northwest. J Geophys Res 109:B08204

Candela, P.A., 1992, Controls on ore metal ratios in granite-related ore systems: An experimental and computational approach: Royal Society of Edinburgh Transactions, Earth Sciences, v. 83, p. 317–326.

Carlson, R.W., and Hart, W.K., 1987. Crustal genesis on the Oregon Plateau. Journal of Geophysics Research 92, 6191–6206.

Chiaradia, M., 2014. Copper enrichment in arc magmas controlled by overriding plate thickness. Nat. Geosci. 7, 43–46.

Coats, R.R., 1987, Geology of Elko County., Nevada: Nevada Bureau of Mines and Geology Bulletin. 101.

Core, D.P., Kesler, S.E., Essene, E.J., Dufresne, E.B., Clarke, R., Arms, D.A., Walko, D., Rivers, M.L., (2005) Copper and Zinc in silicate and oxide minerals in igneous rocks from the Bingham – Park city belt, Utah: synchrotron X-ray-fluorescene data. The Canadian Mineralogist. Vol. 43, pp. 1781-1796.

Damman, A.H., Kars, S.M., Touret, J.L.R., Rieffe, E.C., Kramer, J., Vis, R.D., and Pintea, I., 1996, PIXE and SEM analyses of fluid inclusions in quartz crystals from the K-alteration zone of the Rosia Poieni porphyry-Cu deposit, Apuseni mountains, Rumania: European Journal of Mineralogy, v. 8, p. 1081–1096.

De Hoog, J.C.M., Mason, P.R.D., van Bergen, M.J., (2001) Sulfur and chalcophile elements in subduction zones: constraints from a laser ablation ICP-MS study of melt inclusions from Galunggung Volcano, Indonesia. Geochim Cosmochim Acta 65:3147-3164

Dekov, V.M., Rouxel, O., Asael, D., Halenius, U., Munnik, F., 2013. Native Cu from the oceanic crust: isotopic insights into native metal origin. Chem. Geol. 359, 136–149.

Doe, B.R., (1994) Zinc, copper, and lead in mid-ocean ridge basalts and the source rock control on Zn/Pb in ocean-ridge hydrothermal deposits. Geochim Cosmochim Acta 58:2215-2223

Dold, B., Wade, C. and Fontbote, L., 2009. Water management for acid mine drainage control at the polymetallic Zn– Pb–(Ag–Bi–Cu) deposit Cerro de Pasco, Peru. J. Geochem. Explor, 100, 33–141.

Ehrlich, S., Butler. I., Haliez, L., Rickard, D., Oldroyd, A., and Matthews, A., 2004, Experimental study of the copper isotope fractionation between aqueous Cu(II) and covellite, CuS. Chemical Geology, Vol. 209, pp. 259-269.

Eldholm, O., Thiede, J., Taylor, E., et al., 1989 21: Native Copper in ODP site 642 Tholeiites: *Proceedings of the Ocean Drilling Program, Scientific Results,* Vol. 1

Faure K, Matsuhisa Y, Metsugi H, Mizota C (2002) The Hishikari Au-Ag epithermal deposit, Japan: oxygen and hydrogen isotope evidence in determining the source of paleohydrothermal fluids. Econ Geol 97: 481–498

Fedo, C.M., Nesbitt, H.W., Young, G.M., 1995. Unravelling the effects of potassium metasomatism in sedimentary rocks and paleosols, with implications for paleoweathering conditions and provenance. Geology 23, 921–924.

Fellows, S.A., Canil, D., 2012. Experimental study of the partitioning of Cu during partial melting of Earth's mantle. Earth Planet. Sci. Lett. 337–338, 133–143.

Fouch, M.J., 2012, The Yellowstone Hotspot: Plume or Not? Geology,GMY,aMy 2a0y120;1v2. 40; no. 5; p. 479–480; doi: 10.1130/focus052012.1.

Fulignati P, Sbrana A (1998) Presence of native gold and tellurium in the active high-sulfidation hydrothermal system of the La Fossa volcano (Vulcano, Italy). J Volc Geotherm Resc 86:187-198.

Gale, N.H., Woodhead, A., Stos-Gale, Z.A., Walder, A., Bowen, I., 1999. Natural variations detected in the isotopic composition of copper: possible applications to archaeology and geochemistry. Intern. J. Mass Spectrom. 184, 1–9.

Geist, D., and Richards, M., 1993, Origin of the Columbia Plateau and Snake River plain: Deflection of the Yellow- stone plume: Geology, v. 21, p. 789–792, doi: 10.1130/0 091-7613(1993)021<0789:OOTCPA>2.3.CO;2.

"Geological Survey of Japan, AIST｜産総研地質調査総合センター / Geological Survey of Japan, AIST." Geological Survey of Japan, AIST｜産総研地質調査総合センター / Geological Survey of Japan, AIST. Web. 09 Aug. 2016.

Gill, Robin. *Igneous Rocks and Processes: A Practical Guide.* Chichester, West Sussex, UK: Wiley-Blackwell, 2010. Print.

Graham, S., Pearson, N., Jackson, S., Griffin, W., O'Reilly, S.Y., 2004. Tracing Cu and Fe from source to porphyry: in situ determination of Cu and Fe isotope ratios in sulfides from the Grasberg Cu–Au deposit. Chemical Geology 207 (3–4), 147–169.

Hamlyn, P.R., Keays, R.R., Cameron, W.E., Crawford, A.J., Waldron, H.M., 1985. Pre- cious metals in magnesian low-Ti lavas: implications for metallogenesis and sul- fur saturation in primary magmas. Geochim. Cosmochim. Acta 49, 1797–1811.

Hanan, BB Shervais, JW, and Vetter, SK, 2008, Yellowstone plume-continental lithosphere interaction beneath the Snake River Plain, *Geology,* v. 36, 51-54. DOI: 10.1130/G23935A.1

Hart, WK., and Carlson, R.W., 1985, Distribution and geochronology of Steens Mountain-type basalts from the northwestern Great Basin: Iso. /West, v. 43, p. 5-10.

Hasten, ZEL (2012) Mid-Miocene magmatism in the Owyhee Mountains, ID: origin and petrogenesis of volcanic rocks in the Silver City district. [M.S. thesis] Manhattan, Kansas State University, 222 pp.

Hayashi K, Maruyama T, Satoh H (2000) Submillimeter scale variation of oxygen isotopes of vein quartz at the Hishikari Deposit, Japan. Resource Geol 50:141–150

Heinrich CA, Driesner T, Stefansson A, Seward TM (2004) Magmatic vapor contraction and the transport of gold from the porphyry environment to epithermal ore deposits. Geol 32:761-764.

Heinrich, C.A., 2005, The physical and chemical evolution of low- to medium-salinity magmatic fluids at the porphyry to epithermal transition: A thermodynamic study: Mineralium Deposita, v. 39, p. 864–889.

Heinrich, C.A., Günther, D., Audétat, A., Ulrich, T., and Frischknecht, R., 1999, Metal fractionation between magmatic brine and vapor, determined by microanalysis of fluid inclusions: Geology, v. 27, p. 755–758.

Helz, G.R.,Charnock, J.M., Vaughan, D.J., Garner, C.D., (1993) Multinuclearity of aqueous copper and zinc bisulfide complexes: An EXAFS investigation. Geochim Cosmochim Acta 57:15-25.

Hofmeister A.M., Rossman G.R. (1985) Exsolution of metallic copper from Lake County labradorite. Geology, Vol. 13, No. 9, pp. 644–647, http://dx.doi.org/10.1130/0091-7613(1985)13644:EOMCFL2.0.CO;2.

Irvine, T.N., and Baragar, W.R.A., 1971, A guide to the chemical classification of the common volcanic rocks: Canadian Journal of Earth, v. 8, no. 5, p. 523-548.

Jiang, S., Woodhead, J., Yu, J., Pan, J., Liao, Q., Wu, N., 2002. A reconnaissance study of Cu isotopic compositions of hydrothermal vein-type copper deposit, Jinman, Yunan, China. Chinese Science Bulletin 47 (3), 247–250.

John DA, Hofstra AH, Fleck RF, Brummer JE, Saderholm EC (2003) Geologic setting and

genesis of the Mule Canyon low-sulfidation epithermal gold-silver deposit, North-Central Nevada. Econ Geol 98:425–463

Kamenov G.D., Saunders J.A., Hames W.E., Unger D (2007) Mafic magmas as sources for gold in middle-Miocene epithermal deposits of north- ern Great Basin, USA: evidence from Pb isotopic compositions of native gold. Econ Geol 102:1191–1195.

Kelbert, A., Egbert, G.D., and deGroot-Hedlin, C., 2012, Crust and upper mantle electrical conductivity beneath the Yellowstone Hotspot Track: Geology, v. 40, p. 447–450, doi:10.1130/G32655.1.

Klein, E.M., Karsten, J.L., 1995. Ocean-ridge basalts with convergent-margin geo- chemical affinities from the Chile Ridge. Nature 374, 52–57.

Kogiso, T., Tatsumi, Y., Nakano, S., 1997. Trace element transport during dehydration processes in the subducted oceanic crust: 1. Experiments and implications for the origin of ocean island basalts. Earth Planet. Sci. Lett. 148, 193–205.

Larson, P., Maher, K., Ramos, F., Change, Z., Gasper, M., and Meinert, L., 2003, Cu isotope ratios in magmatic and hydrothermal ore-forming environments. Chemical geology, Vol. 201, pp. 337-350.

Leavitt, E.D., Spell, T.L., Goldstrand, P.M., Arehart, G.B., 2004, Geochronology of the Midas Low-Sulfidation Epithermal Gold-Silver Deposit, Elko County, Nevada. Economic Geology. Vol. 99, pp. 1665-1686.

Lee, C.-T.A., Luffi, P., Chin, E.J., Bouchet, R., Dasgupta, R., Morton, D.M., Le Roux, V., Yin, Q.-Z., Jin, D., 2012. Copper systematics in arc magmas and implications for crust–mantle differentiation. Science 336, 64–68.

Leeman, W.P., 1982a, Development of the Snake River Plain-Yellowstone Plateau province, Idaho and Wyoming: an overview and petrologic model, in Bill Bonnichsen and R. M. Breckenridge, editors, Cenozoic Geology of Idaho: Idaho Bureau of Mines and Geology Bulletin 26.

Leeman, W.P., 1982b, Olivine tholeiitic basalts of the Snake River Plain, Idaho, *in* Bill Bonnichsen and R. M. Breckenridge, editors, Cenezoic Geology of Idaho: Idaho Bureau or Mines and Geology Bulletin 26, p. 181-191.

Lehnert, K., Su, Y., Langmuir, C., Sarbas, B., & Nohl, U. A global geochemical database structure for rocks. *Geochem. Geophys. Geosyst.* 1, doi:10.1029/1999GC000026 (2000)

LeMaitre, R.W., 1976, Some problems of the projection of chemical data into mineralogical classifications, Contributions to mineralogy and Petrology, v. 56, p. 181-189.

Li, W.Q., Jackson, S.E., Pearson, N.J., Alard, O., Chappell, B.W., 2009. The Cu isotopic signature of granites from the Lachlan fold belt, SE Australia. Chem. Geol. 258, 38–49.

Liu, S-A., Huang, J., Liu, J., Wörner, G., Yang, W., Tang, Y-J., Chen, Y., Tang, L., Zheng, J., Li, S., 2015, Copper isotopic composition of the silicate Earth. Earth and Planetary Science Letters 427, pp. 95-103.

Liu, S.-A., Li, D.-D., Li, S.-G., Teng, F.-Z., Ke, S., He, Y.-S., Lu, Y.-H., 2014. High- precision copper and iron isotope analysis of igneous rock standards by MC- ICP-MS. J. Anal. At. Spectrom. 29, 122–133.

Luck, J.M., Ben Othman, D., Barrat, J.A., Albarede, F., (2003) Coupled 63Cu and 18O excesses in chondrites. Geochim Cosmochim Acta 67:143-151

Maréchal, C., Albarede, F., (2002) Ion-exchange fractionation of copper and zinc isotopes. Geochim Cosmochim Acta 66:1499-1509

Maréchal, C.N., Télouk, P., Albarède, F., 1999. Precise analysis of copper and zinc isotopic compositions by plasma-source mass spectrometry. Chemical Geology 156 (1–4), 251–273.

Markl, G., Lahaye, Y., and Schwinn, G., 2006, Copper isotopes as monitors of redox processes in hydrothermal mineralization. Geochimica Cosmochimica Acta, Vol. 70, pp. 4215-4228.

Maher, K.C., and Larson, P.B., 2007, Variation in copper isotope ratios and controls on fractionation in hypogene skarn mineralization at Coroccohuayco and Tintaya, Peru: Economic Geology, v. 102, p. 225−237.

Mason, M., 2015, Ore Petrography, Geochemistry, and Genesis of Epithermal Silver-Gold Veins on Florida Mountain, Silver City District, Idaho [M.S. Thesis] Auburn University.

Mathur, R., Titley, S. R., Schlitt, W. J., Wilson, M., 2012, Cu isotope fractionation in exploration geology and hydrometallurgy examples from porphyry copper deposits. Mining Engineering, Vol. 64, pp. 42.

Mathur, R., Dendas, M., Titley, S., and Philips, A., 2010, Patterns in the copper isotopic composition of minerals in porphyry copper deposits in the southwestern United States of America. Economic Geology. Vol. 105, pp. 1457-1467.

Mathur, R. et al., 2009, Exploration potential of Cu isotope fractionation in porphyry copper deposits: Journal of Geochemical Exploration, v. 102, p. 1-6.

Mathur, R., Ruiz, J., Titley, S., Buss, Heather, Liermann, L., and Brantley, S., 2005, Cu isotope fractionation in the supergene with and without microorganisms. Geochimica et Cosmochimica Acta, Vol. 69, pp. 5233-5246.

Matsuhisa Y, Aoki M (1994) Temperature and oxygen isotope variations during formation of the Hishikari epithermal gold-silver veins, southern Kyushu, Japan. Econ Geol 89:1608–1613

Meeker KA, Chuan RL, Kyle PR, Palais JM (1991) Emission of elemental gold particles from Mount Erebus, Ross Island, Antarctica. Geoph Res Lett 18:1405-1408.

Miller, D.M., Clark, D.L., Wells, M.L., Oviatt, C.G., Felger, T.J., and Todd, V.R., 2012, Progress report geologic map of the Grouse Creek 30’ x 60’ quad. and UT part of the Jackpot 30’ x 60’ quad., Box Elder Co., UT, and Cassia Co., ID: UT Geology Survey OFR-598, 25p.

Moeller, K., Schoenberg, R., Pedersen, R.-B., Weiss, D., Dong, S., 2012. Calibration of the new certified reference materials ERM-AE633 and ERM-AE647 for cop- per and IRMM-3702 for zinc isotope amount ratio determinations. Geostand. Geoanal. Res. 36, 177–199.

Mote, T.I., Brimhall, G.H., Tidy-Finch, E., Muller, G. and Carrasco, P., 2001. Application of mass-balance modeling of sources, pathways, and sinks of supergene enrichment to exploration and discovery of the Quebrada Turquesa exotic copper orebody, El Salvador district, Chile. Econ. Geol, 96, 367–386.

Mungall, J.E., 2002. Roasting the mantle: slab melting and the genesis of major Au and Au-rich Cu deposits. Geology 30, 915–918.

Nesbitt, H.W., Wilson, R.E., 1992. Recent chemical weathering of basalts. Am. J. Sci. 292, 740–777.

O'Neil JR, Silberman ML, Fabbi BP, Chesterman CW (1973) Stable isotope and chemical relations during mineralization in the Bodie Mining District, Mono County, California. Econ Geol 68:765–784

O'Nions, K., Zhu, X., 2002. Natural and experimental mass fractionation of transition metal isotopes. Proceedings of the Goldschmidt-Confer- ence, Geochim. Cosmochim. Acta 66, 15A, A563.

Perkins ME, Nash BP (2002) Explosive silicic volcanism of the Yellowstone Hotspot; the ash fall tuff record. Geol Soc Amer Bull 114:367–381

"PetDB, the Petrological Database." IEDA: EarthChem Homepage. Web. 09 Aug. 2016

Pierce, K.L., and Morgan, L.A., 2009, Is the track of the Yellowstone hotspot driven by a deep mantle plume? Review of volcanism, faulting, and uplift in light of new data: Journal of Volcanology and Geothermal Research, v. 188, p. 1–25, doi:10.1016/j.jvolgeores.2009.07.009.

Plank, T., Langmuir, C.H., 1998. The chemical composition of subducting sediment and its consequences for the crust and mantle. Chem. Geol. 145, 325–394.

Ponce, D.A., and Glen, J.M.G., 2002, Relationship of Epithermal Gold Deposits to Large-Scale Fractures in Northern Nevada: Economic Geology. Vol. 97, pp 3-9.

Pribil, M.J., Wanty, R.B., Ridley, W.I., Borrok, D.M., 2009. Influence of sulfur-bearing polyatomic species on high precision measurements of Cu isotopic composition. Chemical Geology, 272(1-4): 49-54.

Rahl, JM., Foland, KA., and McGrew, AJ., 2002, Transition from contraction to extension in the northeastern Basin and Range; new evidence from the Copper Mountains., Nevada: Journal of Geology, v. 110, p. 179-194.

Richards JP (2009) Post-subduction porphyry Cu-Au and epithermal Au deposits: products of remelting of subduction-modified lithosphere. Geology 37:247–250

Richards, J.P., 2003, Tectono-magmatic precursors for porphyry Cu-(Mo-Au) deposit formation: Economic Geology and the Bulletin of the Society of Economic Geologists, v. 96, p. 1515–1533.

Ringwood, A.E., 1977, Petrogenesis in island arc systems, *in* Talwani, M., and Pitman, W.C., eds., Island arcs, deep sea trenches, and back arc basins: American Geophysical Union Maurice Ewing Series I, p. 311–324.

Riuz, J., Mathur, R., Young, S., Brantley, S., 2002. Controls of copper isotope fractionation. Proceedings of the Goldschmidt-Conference, Geochim. Cosmochim. Acta 66, 15A, A484.

Robb, L., 2005. Introduction to Ore- Forming Processes. Blackwell Scientific Publication, Oxford.

Rouxel, O., Fouquet, Y., Ludden, J.N., 2004. Copper isotope systematics of the Lucky Strike, Rainbow, and Logatchev sea-floor hydrothermal fields on the Mid-Atlantic Ridge. Economic Geology and the Bulletin of the Society of Economic Geologists 99 (3), 585–600.

Russell S.S., Zhu, X., Guo, Y., Belshaw, N., Gounelle, M., Mullane, E., (2003) Copper isotope systematics in CR, CH-like, and CB meteorites: a preliminary study (abst). Meteorit Planet Chem Geol, 38.

Saunders JA, Brueseke ME (2012) Volatility of metal(loids) and the geo- chemistry of epithermal Au-Ag ores in western USA. Econ Geol 107:165–172

Saunders, J.A., Unger, D.L., Kamenov, G.D., Fayek, M., Hames, W.E., and Utterback, W.C., 2008, Genesis of mid-Miocene Yellowstone-hotspot-related bonanza epithermal Au-Ag deposits, Northern Great Basin Region, USA: *Mineralium Deposita*, v. 43, no. 7, p. 715-734.

Saunders, J.A., Mathur, R., Mathur, R., Kamenov, G.D., Shimizu, T., Brueseke, M.E., 2015, New isotopic evidence bearing on bonanza (Au-Ag) epithermal ore-forming processes. Miner. Deposita.

Savage, P., Chen, H., Shofner, G., Badro, J., Moynier, F., 2013. The copper isotope composition of bulk Earth: a new paradox. Goldschmidt abstracts, P2142.

Seo, J.H., Lee, S.K., Lee, I., 2007. Quantum chemical calculations of equilibrium copper (I) isotope fractionations in ore-forming fluids. Chemical Geology 243 (3–4), 225–237

Shields W.R., Murphy, T.J., Garner, E.L, (1964) Absolute Isotopic abundance ratio and the atomic weight of a reference of copper. J Res NBS 68A:589-592.

Sillitoe, R.H., (1972) A plate tectonic model for the origin of porphyry copper deposits. Econ Geol 67:184-197.

Sillitoe, R.H., 2010. Porphyry copper systems. Econ. Geol., 105, 3–41.

Simmons SF, White NC, John DA (2005) Geological characteristics of epithermal precious and base metal deposits. 100th Anniv Vol Econ Geol 485-522

Smith, R.B., and Braile, L.W., 1994, The Yellowstone Hotspot: Journal of Vol- canology and Geothermal Research, v. 61, p. 121–187, doi:10.1016/0377 -0273(94)90002-7.

Stolper, E., Newman, S., (1994) The role of water in the petrogenesis of Mariana trough magmas. Earth Planet Sci Lett 121:293-325.

Takano, S., Tanimizu, M., Hirata, T., Sohrin, Y., 2013. Determination of isotopic composition of dssolved copper in seawater by multi-colector inductively coupled plasma mass spectrometry after pre-concentration using an ethylenediaminetriacetic acid chelating resin. Anal. Chim. Acta 784, 33–41.

Taran YA, Bernard A, Gavilanes JC, Africano F (2000) Native gold in mineral precipitates from high-temperature volcanic gases of Colima volcano, Mexico. Appl Geochem 15: 337–346.

Thompson, C.M., Ellwood, M.J., Wille, M., 2013. A solvent extraction technique for the isotopic measurement of dissolved copper in seawater. Anal. Chim. Acta 775, 106–113.

Titley, S.R., 1982. The style and progress of mineralization and alteration in porphyry copper systems; American Southwest. Advances in geology of porphyry copper deposits; southwestern North America. Univ. Ariz. Press, Tucson, AZ, pp. 93–116.

Titley, S.R. and Beane, R.E., 1981. Porphyry copper deposits: part I. Geologic settings, petrology, and tectogenesis. Econ. Geol., 75, 214–235.

Titley, S.R. and Marozas, D., 1995. Processes and products of supergene copper enrichment. In: Advances in Geology of the Porphyry Copper Deposits, Southwestern North America (S. Titley, ed.), pp. 156–168. University of Arizona Press, Arizona.

Ulrich, T., Günther, D., and Heinrich, C.A., 1999, Gold concentrations of magmatic brines and the metal budget of porphyry copper deposits: Na- ture, v. 399, p. 676–679.

"U.S. Geological Survey." USGS.gov |. Web. 09 Aug. 2016.

Vance, D., Archer, C., Bermin, J., Statham, P., Lohan, M., Ellwood, M., Mills, R., 2008. The copper isotope geochemistry of rivers and the oceans. Earth Planet. Sci. Lett. 274, 204–213.

Wall, A.J., Mathur, R., Post, J.E., and Hearney, P.J., (2011) Cu isotope fractionation during bornite dissolution: An in situ X-ray diffraction analysis: Ore Geology Reviews, v. 42, 62-70.

Williams-Jones A.E., and Heinrich, C.A. (2005) Vapor transport of metals and the formation of magmatic-hydrothermal ore deposits. Econ Geol 100:1287-1312.

Yudovskaya M.A., Distler V.V., Chaplygin I.V. (2006) Gaseous transport and deposition of gold in magmatic fluid: evidence from the active Kudryavy volcano, Kurile Islands. Miner. Deposita. 40:828–848.

Zhu, X., Gou, Y., Willimas, R.J.P., O'Nions, R.K., Matthews, A., Belshaw, N.S., Canters, G.W., de Waal, E.C., Weser, U., Burgess, B.K., and Salvato, B., (2002) Mass fractionation process of transition metal isotopes. Earth and Planetary Science Letters. Vol. 200, pp. 47-62.

Zhu, X.K., O'Nions, R.K., Guo, Y., Belshaw, N.S., Rickard, D., 2000. Determination of natural Cu-isotope variation by plasma-source mass spectrometry: implications for use as geochemical tracers. Chem. Geol. 163, 139–149.

Appendix A - Sample Locations and Petrographic Descriptions

Locations presented in UTM coordinates are based off the NAD27 CONUS datum. Rock type classifications are based on total alkali vs. silica classification from LeBas et. al. 1986. Descriptions contain field, hand sample and thin section information.

Sample ID: JC-09-20 **Easting:** 0598310
Rock Type: Basaltic andesite **Northing:** 4625109

Description: Holocrystalline with crystalline groundmass. Phenocrysts include three populations of plagioclase by size fractionation. The largest population is euhedral and partially sieved, the next smallest population is subhedral and sieved, and the groundmass population is subhedral. Anhedral titanaugite and subhedral olivine also occur.

Sample ID: AM15-3 **Easting:** 0671882
Rock Type: Basalt **Northing:** 4747851

Description: Dark grey, porphyritic, hypocrystalline rock. Visible green olivine grains and euhedral plagioclase laths approximately 5mm long. Abundant but scattered olivine-plagioclase intergrowths measuring 3-8mm in length. Plagioclase grains are euhedral and exhibit zoning. Clusters of subhedral olivine grains also abundant measuring approximately 2-5mm in diameter. Matrix is a mixture of fine grained plagioclase grains, anhedral olivine grains and brown/black glassy material.

Sample ID: AM15-4 **Easting:** 0684459
Rock Type: Basalt **Northing:** 4727206

Description: Dark grey fine grained, porphyritic, vesicular rock. Plagioclase laths and green olivine grains visible. Rounded vesicles averaging 3mm in diameter. Fine grained matrix consists of scattered subhedral plagioclase laths with olivine and glassy material filling the interstitial areas. Rounded vesicles range in size from 1mm to 1.5cm and are common among interlocking plagioclase grains. Phenocrysts include euhedral plagioclase laths, some exhibiting sieve textures in their core. Olivine clots abundant and scattered and exhibits a Poikilitic texture with sub- to euhedral magnetite grains.

Sample ID: ZH11-4 **Easting:** 0520668
Rock Type: Trachybasalt **Northing:** 4756681

Description: Fresh basalt unit overlying granitoid, not much weathering rind. Abundant 1-2mm olivine phenocrysts. Fine grained, aphanitic, dark grey, groundmass. 88.16% olivine 8.49%, and brown interstitial 3.35%. Aphanitic groundmass with abundant 0.15mm felty aligned plagioclase laths. Abundant euhedral to subhedral olivine phenocrysts with iddingsite altered rims.

Sample ID: MB00-30B **Easting:** 4624034
Rock Type: Basaltic trachyandesite **Northing:** 453783

Description: Uppermost exposed mafic lava flow. Coarse grained, dark gray matrix with abundant alteration. ~1cm plagioclase phenocrysts present but the flow is not plagioclase-phyric. Numerous amygdaloidal quartz/chalcedony filled vesicles. Small feldspar laths present in matrix.

Sample ID: MB01-12 **Easting:** 4616329
Rock Type: Basalt **Northing:** 451323

Description: Mafic lava flow that overlies baked tuffaceous material and siliceous sinter. ~3 - 4 m thick with tortoise shell fracturing. Dark gray/blue very sugary fine-grained matrix. Abundant plagioclase laths (1 - 3 mm) and red/black ophiomottling. Holocrystalline, ophitic to subophitic clinopyroxene and plagioclase. One large resorbed plagioclase (up to 2 mm) present; composition is An_{65}. Plagioclase up to 2 mm (composition varies between An_{46} to An_{60}), olivine up to 0.5 mm, oxides, clinopyroxene, apatite and "clay" in matrix.
Mode: Plagioclase 56.83%; oxides 7.25%; olivine 14.50%; clinopyroxene 15.83%; resorbed plagioclase crystal 1.16%; matrix 4.42%.

Sample ID: MB97-31 **Locality:** Route 78 north
Rock Type: Basalt

Description: Plagioclase-phyric lava flow, similar to MB97-30. Slight columnar jointing starting to become present and abundant vesicle trains/pipes. Open textured, gray medium grained matrix plagioclase phenocrysts up to 3 cm long and 2 cm wide. Olivine microphenocrysts also present.

Sample ID: MB97-74B **Locality:** Miranda Flat
Rock Type: Trachybasalt

Description: From within basal section of MB97-74 flow. Blocky chunks of fine, dark matrix material. Appears to be basal rubble zone breccia. Heterolithologic; some of these clasts are plagioclase phyric, some are olivine rich, some aphyric.

Sample ID: MB97-71 **Locality:** Miranda Flat
Rock Type: Basalt

Description: Vesicular top with a massive interior. Flow is ~15' thick. Sampled above basal rubble zone. Fine grained, open-textured dark gray matrix. Microphenocrysts of plagioclase and olivine also present. Massive outcrop with platy fractures and vertical jointing.

Sample ID: MB97-80 **Locality:** Miranda Flat
Rock Type: Basalt trachyandesite

Description: 10' thick flow. Massive and vesicular in places; sparkly textured. Fine grained, dark matrix with plagioclase in the matrix. No noticeable olivine and possibly some pyroxene.

Sample ID: MB09-13 **Easting:** N/A
Rock Type: Basalt **Northing:** N/A

Description: Medium grained equigranular rock. Abundant scattered plagioclase laths interlocking with one another. Anhedral olivine grains present in between plagioclase laths. Extensive weathering of olivine to iddingsite. Euhedral to subhedral magnetite grains present in the interstitial material along with glassy matrix.

Sample ID: MB09-29 **Easting:** N/A
Rock Type: Basalt **Northing:** N/A

Description: Porphyritic rock with 1-2cm plagioclase phenocrysts. Large plagioclase laths with exsolution lamellae exhibit a poikilitic texture with fine grained magnetite. Matrix includes fine grained plagioclase laths, euhedral and needle magnetite grains, olivine grains weathering to iddingsite and green chlorite. Chlorite is also seen as veins (1mm wide) cutting through plagioclase laths and matrix.

Sample ID: 2-12BB **Locality:** Midas, NV
Rock Type: Basaltic andesite

Description: Coarse grained rock with large olivine and plagioclase grains visible. Interlocking plagioclase laths are euhedral and embayed. Olivine grains are subhedral and occur in close association with plagioclase laths. Coarse grained skeletal magnetite grains present between plagioclase and olivine grains. Extensive carbonaceous material present in between grains.

Sample ID: 6-12BB **Locality:** Midas, NV
Rock Type: Basaltic Andesite

Description: Light grey fine grained rock. Abundant scattered plagioclase laths exhibiting exsolution lamellae. Extensive blue/green chlorite present in between plagioclase laths. Fine grained magnetite and carbonaceous material occupy the spaces in between plagioclase grains as well.

Appendix B - Geochemistry

All major and trace element data reported in this appendix are raw unnormalized data. Major elements are reported in wt. % oxide and trace elements are reported in ppm. Newly collected samples from summer 2015 are reported first followed by previously collected samples and standards.

Major Element Results (wt. %)

Sample	AM15-3	AM15-4
SiO_2	47.68	47.58
TiO_2	2.99	2.65
Al_2O_3	14.88	14.41
FeO*	13.76	13.37
MnO	0.20	0.20
MgO	7.03	8.31
CaO	9.38	9.12
Na_2O	2.66	2.49
K_2O	0.77	0.80
P_2O_5	0.52	0.45
Total	99.89	99.39
LOI %	0.00	0.00

Trace Element Results (ppm)

Sample	AM15-3	AM15-4
Ni	106	133
Cr	206	244
Sc	28	29
V	286	279
Ba	398	407
Rb	16	18
Sr	318	295
Zr	240	221
Y	39	35
Nb	20.1	19.5
Ga	21	20
Cu	47	45
Zn	142	132
Pb	3	5
La	24	23
Ce	54	63
Th	2	3
Nd	32	33
U	1	0

Major Element results for previously collected NGB samples (wt. % oxide)

Sample	MB00-30 B	MB01-12	MB09-13	MB09-29	ZH11-4	JC-09-20
SiO_2	51.28	47.59	48.92	49.11	48.28	50.36
TiO_2	3.33	1.36	1.91	2.39	2.01	1.9
Al_2O_3	13.97	16.62	15.21	17.07	15.94	15.85
Fe_2O_3	5.24	3.77	3.94	4.21	3.71	2.87
FeO	8	7.39	7.54	8.48	5.81	5.4
MnO	0.2	0.18	0.18	0.19	0	0.19
MgO	3.75	8.64	7.77	4.24	8.34	5.27
CaO	7.11	9.88	10.23	9.93	8.82	8.26
Na_2O	3.44	2.63	2.6	2.3	3.37	2.85
K_2O	1.7	0.33	0.63	0.73	2.09	1.15
P_2O_5	0.65	0.14	0.21	0.4	0.99	0.46
Total	100	100	100	100	100	100
LOI	0.44	0.654	1.55	3.73	1.81	0.66

Major Element results for previously collected NGB samples (wt. % oxide)

Sample	2-12BB	6-12BB	MB97-74B	MB97-71	MB97-80	MB97-31
SiO_2	52.9	51.34	49.4	47.38	55.49	50.37
TiO_2	1.02	0.82	3.19	2.71	1.93	2.22
Al_2O_3	16.74	16.93	14.05	15.5	15.42	17.54
Fe_2O_3	3.11	2.87	15.34	15	9.92	11.7
FeO	5.95	5.4	-	-	-	-
MnO	0.15	0.15	0.22	0.2	0.18	0.16
MgO	7.17	7.31	4.26	5.8	2.95	4.26
CaO	8.48	11.22	7.73	8.63	5.78	9.44
Na_2O	2.39	2.46	3.55	3.25	4.17	3.25
K_2O	1.16	0.7	1.67	1.09	2.87	0.82
P_2O_5	0.26	0.21	4.15	3.56	5.17	3.68
Total	100	100	101.18	100.42	99.62	100.13
LOI	8.47	3.68	0.02	0.27	0.68	0.94

Trace and rare earth element results from previously collected NGB samples (ppm)

Sample	MB00-30 B	MB01-12	MB09-13	MB09-29	ZH11-4	JC-09-20	2-12BB	6-12BB
Ba	653	165	180	293	1258	727	352	272
Ce	64	15	25	45	111	83	34	26
Cr	27	102	198	47	205	61	140	360
Cs	-	0.30	0.58	-	-	0.50	2.32	7.12
Dy	-	4.3	5.2	-	-	8.0	4.0	3.6
Er	-	2.29	2.56	-	-	4.56	2.65	2.34
Eu	-	1.31	1.75	-	-	2.37	1.05	1.01
Ga	25.9	18.6	19	23	21	22.0	17.7	16.8
Gd	-	4.07	5.29	-	-	8.78	3.89	3.62
Hf	-	1.96	3.40	-	-	6.82	2.90	2.30
Ho	-	0.87	1.02	-	-	1.58	0.86	0.77
La	33.0	6.3	10.3	19.1	45.3	40.9	16.1	12.4
Lu	-	0.30	0.31	-	-	0.66	0.36	0.32
Nb	24.9	3.2	7.6	13.9	20.9	-	7.6	5.6
Nd	-	11.15	17.27	27	54	40.87	17.9	14.4
Pr	-	2.16	3.70	-	-	9.81	4.36	3.46
Rb	38.2	3.7	13.4	17.0	38.0	11.1	30.9	20.9
Sm	-	3.52	4.83	-	-	9.22	4.00	3.24
Sn	-	-		-	-	1.42	2	1
Sr	410	410	348	444	1505	421	232	292
Ta	-	0.27	0.50	-	-	1.27	0.40	0.30
Tb	-	0.69	0.86	-	-	1.36	0.64	0.58
Th	7.30	0.43	1.06	1.00	6.00	2.62	2.89	2.00

Trace and rare earth element results from previously collected NGB samples (ppm)

Sample	MB00-30 B	MB01-12	MB09-13	MB09-29	ZH11-4	JC-09-20	2-12BB	6-12BB
Tl	-	-	-	-	-	-	<0.5	<0.5
Tm	-	0.32	0.35	-	-	0.64	0.38	0.33
U	2	0.13	0.35	2	3	0.68	0.95	0.64
V	200	261	310	277	214	166	218	210
W	-	-	-	-	-	1.70	<1	<1
Y	32.6	26.9	25.1	31	24	44.9	23.5	19.4
Yb	-	1.91	2.11	-	-	4.45	2.27	2.03
Zr	229	73	128	185	265	281	111	80
As	-	-	-	-	-	3.7	5.4	2.0
Bi	-	-	-	-	-	-	0.08	0.04
Hg	-	-	-	-	-	-	0.22	0.09
Sb	-	-	-	-	-	0.04	2.0	0.7
Se	-	-	-	-	-	-	0.8	0.5
Sc	22	26	29	24	21	32	22	27
Te	-	-	-	-	-	-	0.01	<0.01
Ag	-	-	-	-	-	-	<0.5	<0.5
Cd	-	-	-	-	-	-	<0.5	<0.5
Co	34	54	-	-	-	45	34	35
Cu	239	135	168	63	47	36	220	99
Li	-	-	-	-	-	2.9	160	10
Mo	-	-	-	-	-	1.01	<1	<1
Ni	28	150	177	67	142	35	61	67
Pb	34	0.98	2.12	3.00	9.00	2.33	8.00	3.00
Zn	97	82	93	121	117	137	95	78

Trace and rare earth element results from previously collected NGB samples (ppm)

Sample	MB97-74B	MB97-71	MB97-80	MB97-31
Ba	619	441	1023	394
Ce	61	37	75	36
Cr	22	28	13	48
Cs	5.8	5.5	7.6	3.4
Dy	-	-	-	-
Er	-	-	-	-
Eu	272	205	253	116
Ga	27.8	26.2	23.3	26.6
Gd	-	-	-	-
Hf	-	-	-	-
Ho	-	-	-	-
La	32.7	20.6	34.8	16.7
Lu	-	-	-	-
Nb	17.7	14.0	15.7	12.9
Nd	46	37	38	26
Pr	-	-	-	-
Rb	30.0	16.8	54.4	6.9
Sm	-	-	-	-
Sn	-	-	-	-
Sr	444	471	701	462
Ta	-	-	-	-
Tb	-	-	-	-
Th	5.8	5.5	7.6	3.4

Trace and rare earth element results from previously collected NGB samples (ppm)

Sample	MB97-74B	MB97-71	MB97-80	MB97-31
Tl	-	-	-	-
Tm	31.30	27.10	17.60	28.30
U	1.30	1.20	1.40	0.30
V	463	389	172	334
W	-	-	-	-
Y	46.0	36.5	37.9	26.2
Yb	-	-	-	-
Zr	272	205	253	116
As	-	-	-	-
Bi	-	-	-	-
Hg	-	-	-	-
Sb	-	-	-	-
Se	-	-	-	-
Sc	31.3	27.1	17.6	28.3
Te	-	-	-	-
Ag	-	-	-	-
Cd	-	-	-	-
Co	40	50	23	38
Cu	414.0	283.9	46.5	116.8
Li	-	-	-	-
Mo	-	-	-	-
Ni	49	110	7.1	143
Pb	8.0	5.1	11	4.1
Zn	135	126	139	102

Major element data results from international rock standards (wt. % oxide)

Sample	AGV-1	BCR-2	JB-1a	JB-3	PCC-1	JA-3
SiO_2	58.84	54.11	52.16	51.04	41.71	62.26
TiO_2	1.05	2.24	1.3	1.45	0.01	0.68
Al_2O_3	17.15	13.64	14.51	16.89	0.68	15.57
$Fe_2O_3^T$	6.77	13.41	9.1	11.88	8.25	6.59
MnO	0.09	0.18	0.15	0.16	0.12	0.11
MgO	1.53	3.48	7.75	5.2	43.43	3.65
CaO	4.94	6.95	9.23	9.86	0.52	6.28
Na_2O	4.26	3.27	2.74	2.82	0.03	3.17
K_2O	2.92	1.69	1.42	0.78	0.007	1.41
P_2O_5	0.49	0.36	0.26	0.29	0.002	0.11
Total	97.96	99.28	98.62	100.37	94.71	99.83

Major element data results from international rock standards (wt. % oxide)

Sample	JA-2	JB-2	BHV0-1	DNC-1	JGb-1	BE-N
SiO_2	56.18	53.2	49.94	47.04	43.44	38.2
TiO_2	0.67	1.19	2.71	0.48	1.62	2.61
Al_2O_3	15.32	14.67	13.8	18.3	17.66	10.07
$Fe_2O_3^T$	6.14	14.34	12.23	9.93	15.16	12.84
MnO	0.11	0.2	0.17	0.15	0.17	0.2
MgO	7.68	4.66	7.23	10.05	7.83	15
CaO	6.48	9.89	11.4	11.27	11.98	13.87
Na_2O	3.08	2.03	2.26	1.87	1.23	3.18
K_2O	1.8	0.42	0.52	0.23	0.24	1.39
P_2O_5	0.15	0.1	0.273	0.09	0.05	1.05
Total	97.61	100.7	100.53	99.4	99.38	96.56

Trace and rare earth element results from international rock standards (ppm)

Sample	AGV-1	BCR-2	JB-1a	JB-3	PCC-1	JA-3
Ba	1226	681	497	251	1.2	318
Ce	67	54	66	22	0.1	23
Cr	10	16	415	60	2730	68
Cs	-	-	-	-	-	-
Dy	3.60	6.34	4.19	4.55	0.01	2.97
Er	1.7	3.63	2.18	2.61	0.01	1.46
Eu	1.64	1.95	1.47	1.31	0.002	0.85
Ga	-	-	-	-	-	-
Gd	5.00	6.68	4.54	4.47	0.01	2.94
Hf	5.1	4.95	3.48	2.68	0.04	3.43
Ho	-	-	-	-	-	-
La	-	-	-	-	-	-
Lu	0.27	0.51	0.32	0.39	0.01	0.32
Nb	15	14	27	2.3	1.0	3.0
Nd	33.0	28.8	25.5	15.4	0.04	12.3
Pr	-	-	-	-	-	-
Rb	67.3	47.2	41.0	13.0	0.1	36.0
Sm	5.90	6.59	5.07	4.27	0.01	3.14
Sn	-	-	-	-	-	-
Sr	662	330	443	395	0.4	294
Ta	-	-	-	-	-	-
Tb	-	-	-	-	-	-
Th	6.5	5.9	8.8	1.3	0.01	3.4

Trace and rare earth element results from international rock standards (ppm)

Sample	AGV-1	BCR-2	JB-1a	JB-3	PCC-1	JA-3
Tl	-	-	-	-	-	-
Tm	-	-	-	-	-	-
U	-	-	-	-	-	-
V	121	407	220	383	31	172
W	-	-	-	-	-	-
Y	20	38	24	27	0.1	21
Yb	1.72	3.38	2.10	2.62	0.02	2.18
Zr	227	190	146	98	10	119
As	-	-	-	-	-	-
Bi	-	-	-	-	-	-
Hg	-	-	-	-	-	-
Sb	-	-	-	-	-	-
Se	-	-	-	-	-	-
Sc	12.2	32.6	27.9	33.3	8.4	21.8
Te	-	-	-	-	-	-
Ag	-	-	-	-	-	-
Cd	-	-	-	-	-	-
Co	-	-	-	-	-	-
Cu	60	19	56	198	10	45
Li	-	-	-	-	-	-
Mo	-	-	-	-	-	-
Ni	16	13	140	39	2380	36
Pb	36	14	7.2	5.5	10	6.7
Zn	88	130	82	106	42	68

Trace and rare earth element results from international rock standards (ppm)

Sample	JA-2	JB-2	BHV0-1	DNC-1	JGb-1	BE-N
Ba	317	208	139	114	63	1025
Ce	33	6.8	39	11	7.9	152
Cr	465	27	289	285	59	360
Cs	-	-	-	-	-	-
Dy	3.01	3.66	5.20	2.70	1.53	6.40
Er	1.37	2.63	2.40	2.00	1.07	2.50
Eu	0.94	0.86	2.06	0.59	0.63	3.60
Ga	-	-	-	-	-	-
Gd	3.11	3.28	6.40	2.00	1.63	9.70
Hf	2.89	1.42	4.38	1.01	0.88	5.60
Ho	-	-	-	-	-	-
La	-	-	-	-	-	-
Lu	0.27	0.32	0.29	0.32	0.15	0.24
Nb	9.8	0.8	19	3.0	2.8	105
Nd	13.8	6.7	25.2	4.9	5.7	67.0
Pr	-	-	-	-	-	-
Rb	68	6.2	11	4.5	4.0	47
Sm	3.12	2.25	6.20	1.38	1.49	12.20
Sn	-	-	-	-	-	-
Sr	252	178	403	145	321	1370
Ta	-	-	-	-	-	-
Tb	-	-	-	-	-	-
Th	4.70	0.33	1.08	0.20	0.53	10.40

Trace and rare earth element results from international rock standards (ppm)

Sample	JA-2	JB-2	BHV0-1	DNC-1	JGb-1	BE-N
Tl	-	-	-	-	-	-
Tm	-	-	-	-	-	-
U	-	-	-	-	-	-
V	130	578	317	148	640	235
W	-	-	-	-	-	-
Y	18.1	24.9	27.6	18.0	10.8	30.0
Yb	1.67	2.51	2.02	2.01	0.97	1.8.0
Zr	119	51	179	41	34	260
As	-	-	-	-	-	-
Bi	-	-	-	-	-	-
Hg	-	-	-	-	-	-
Sb	-	-	-	-	-	-
Se	-	-	-	-	-	-
Sc	19.6	54.4	31.8	31.0	36.6	22.0
Te	-	-	-	-	-	-
Ag	-	-	-	-	-	-
Cd	-	-	-	-	-	-
Co	-	-	-	-	-	-
Cu	29	227	136	96	87	72
Li	-	-	-	-	-	-
Mo	-	-	-	-	-	-
Ni	142	14	121	247	25	267
Pb	19	5.4	2.6	6.3	1.9	4.0
Zn	63	110	105	66	111	120